Synchronized Temporal-spatial Analysis via Microscopy and Phoshoproteomics (STAMP) of Quiescence

Mohammad Ovais Aziz-Zanjani,[1,2] Rachel E. Turn,[1,2] Lucy Artemis Xu,[1] Peter K. Jackson[1,3]

[1] Baxter Laboratory, Department of Microbiology & Immunology, Stanford University School of Medicine, Stanford, CA 94305, USA

[2] Co-first authors who contributed equally to this manuscript

[3] Lead contact: pjackson@stanford.edu

SUMMARY: Tightly coordinated cell cycle regulation is essential for homeostasis. G_0, or quiescence, is especially crucial for cells to respond to extracellular stimuli. Little is known about the mechanisms that establish the G_0 program, though the primary cilium (a key signaling hub formed only in G_0) is the most widely recognized marker. The study of ciliogenesis is challenging due to its small size, relative to the cell body. To address this gap in our understanding, we developed STAMP (Spatio-Temporal Analysis via Microscopy and Proteomics) to temporally map the changes in cellular landscape occurring in G_0 and ciliogenesis. Using synchronized RPE cells, we used fixed and live cell imaging combined with phosphoproteomics to uncover new signals and order them in these processes, which also allows further, more targeted, analyses (e.g., using genetic and pharmacological perturbations). We propose that STAMP is broadly applicable for studying temporal-spatial signaling processes and the underlying mechanisms in various biological contexts and cell types.

KEYWORDS: cell cycle, cilia, ciliogenesis, cytokinesis, G_0, Golgi, kinases, mTOR, mitosis, phosphoproteomics, phosphorylations, proteomics, quiescence, STAMP, synchronization, time-lapse, translational control, vesicular traffic

Fundamental cellular processes are driven by highly coordinated, temporal-spatial regulation of the cell signaling network. Post-translational modifications (PTMs), in particular, allow for rapid cellular responses to environmental cues, as these transient and frequently reversible modifications can alter protein structure, stability, interactions, and localization. The transient nature of PTMs (including phosphorylations, the most widely studied of PTMs) and protein localization underscores the dynamic and reversible nature of cellular regulation. At its core, pathology arises due to the disruption of these critical PTMs and transient, context-specific cellular functions, highlighting the urgent need to dissect these mechanisms. Yet, because much previous studies have relied upon cancer cell lines as model systems for signaling, we have very little insight into the signaling landscape of healthy, quiescent cells, the most prevalent cell cycle status in human organs.[1] Identifying transient phosphorylations that induce or later maintain quiescence (G_0) in noncancerous cells is crucial for advancing cell biology. Yet, mapping the temporal-spatial signaling landscape in healthy, quiescent cells is complicated by

the dearth of quiescent program markers and the lack of tools to track changes in PTMs and protein function in time and space.

One of the few widely accepted hallmarks of quiescence in most cell types is the primary cilium, an organelle that protrudes into the extracellular space and acts as a pivotal signaling hub.[2] This tiny organelle is composed of a mother centriole, called the basal body, that projects a microtubule-based axoneme encased in plasma membrane. The primary cilium houses specific receptors that sense extracellular stimuli and transduce those signals to propagate discrete cellular responses. Disruption of these signals drive a number of severe pathologies, including multi-system developmental disorders called ciliopathies,[3,4] blindness,[5] kidney disorders,[6] diabetes,[7-9] obesity,[10] Parkinson's disease,[11] and cancers.[12]

A significant impediment in studying G_0 transition and ciliary function is the inability to detect transient, context-specific signals in time and space. For example, the standard method to induce ciliogenesis in cultured cells involves seeding at a high density (80-90%) followed by serum starvation for 24-72hrs. However, the lack of synchrony in G_0 entry and initiation of ciliogenesis results in the dilution of transient changes to below limits of detection by either imaging or proteomics. To tackle this challenge, we leveraged the power of state-of-the-art mass spectrometry (MS) and fixed and live-cell imaging to track the temporal-spatial network of proteins and their PTMs in differential signaling contexts. By generating a much more homogeneous cell population, we can clearly correlate changes in cellular processes via microscopy with specific, often transient, PTMs identified via mass spectrometry that together support testable hypotheses regarding mechanisms. Our novel approach for teasing apart subcellular temporal-spatial PTM-driven signaling is termed **STAMP**: **S**ynchronized **T**emporal-spatial **A**nalysis via **M**icroscopy and **P**roteomics. Below, we provide a detailed methodology for applying STAMP to tracking temporal phosphorylations and their correlational effects on the localization and function of these proteins on cytokinesis, nuclear pore complex (NPC) formation, Golgi reorganization, centrosomal maturation, translation, and ciliogenesis from mitosis to G_0 entry in non-cancerous cells. We focus here on our analyses of G_0 and ciliogenesis to demonstrate the value of the methodology, though note that it can be used to dissect and identify key components in many other cellular processes.

RESULTS:

Premise:

Our goal was to develop a method to allow detailed molecular and cellular analyses of distinct stages in the progression of essential processes during the transition from mitosis to G_0 commitment, including but not limited to mitosis, cytokinesis, ciliogenesis, translational control, and vesicular traffic. We used rigorous cell synchronization, followed by multi-dimensional analyses with high temporal resolution over 24hrs. The combination of fixed and live cell imaging with state-of-the-art phosphoproteomics (Fig. 1A) allowed us to perform detailed ordering of cellular events (Fig. 2A). By doing so, we observed strong correlations that suggest testable hypotheses regarding the roles of specific, often transient or rare and previously undetected, phosphorylations in those processes. As our model system, we chose human retinal pigment epithelial cells (RPE) as they are 1)

human, non-cancerous, adherent, mononucleated cells, 2) a commonly used model system for studies of ciliogenesis, and 3) readily tractable for several different methodologies and perturbations.

Generation of synchronized cells

We developed a rigorous approach to synchronize the transition to quiescence using ciliogenesis as a marker of G_0. The established approach for inducing G_0 and ciliation is serum starvation (0-0.5% fetal bovine serum) of cells near confluence (80-90% density). Primary cilia can be identified via immunofluorescence (IF) using antibodies targeting acetylated tubulin to mark the axoneme, ARL13B to mark the ciliary membrane, and Cep170 or centrin to mark the basal body.[13-18] When asynchronous cell populations grown on fibronectin-coated coverslips were switched to serum-free medium, we observed a linear progression of ciliogenesis, with cilia forming as early as 2hrs and gradually increasing to 70-90% ciliated cells over a 24hr window (Fig 1B-C). Note that this standard approach of tracking ciliogenesis only accounts for axoneme extension and lacks data on the timing of earlier licensing events or functionality in receptor recruitment. This asynchronous population of cells undergoing ciliogenesis does not allow tracking or ordering of transient cellular events or linking them to changes in PTMs. Thus, we developed a rigorous, multi-step synchronization protocol to achieve time-resolved differential analysis of the stages of G_0 transition and ciliogenesis.

After optimizing drug concentrations and incubation intervals to maximize cell health, purity, and yield, we developed the following protocol for synchronizing G_0 entry in retinal pigmented epithelial (RPE) cells. Cells were seeded at 10% confluence and then grown in standard growth medium for 24hrs, at which point the cyclin-dependent kinase inhibitor palbociclib (1µg/mL) was added to prevent cells from exiting G_1 (Fig.S1A). After 18hrs, the drug was removed, and the cells were allowed to recover for 8hrs. At this point, the microtubule inhibitor nocodazole (50ng/mL) was added to synchronize the cells at metaphase. After 12hrs, we performed mitotic shake-off to isolate metaphase-synchronized cells, achieving ~30% yield of total cell input. Based on immunostaining, this triple synchronization methodology (double block and shake-off) yields nearly 100% mitosis-synchronized cells (Fig.1B). We then filtered for single cells using a cell strainer and incubated in standard growth medium for 20min at 37°C before plating. This allowed microtubules to recover and ciliogenesis to occur earlier and more synchronously (Fig.S1B). Cells were then plated onto fibronectin-coated coverslips and/or plates in serum-free medium to induce G_0 transition.[19,20] We confirmed a uniquely high degree of synchronization in mitosis and cilia formation, with essentially all cells completing cytokinesis by 2hr and initiating cilia projection within a 2-hour window, occurring 10-12hrs after seeding (Fig.1C,E).

Temporal changes in protein localization reveal stages of quiescent transition.

With evidence that the protocol achieved a high degree of synchronization, cells were fixed for IF every 1-2 hours for 24 hours after recovery from mitotic shake-off to document cellular changes, using previously well-characterized markers. These included: CEP164 and TTBK2 as markers of centrosome maturation; TGN38 and GM130 for Golgi morphology; RAB34 to track vesicle transport to the centrosome; CEP290 to label the transition zones; GPR161, PDGRFα, and ARL13B as representative ciliary membrane proteins; acetylated tubulin to both

identify axonemes and determine cilia lengths; and intraflagellar transport (IFT) components IFT88 to identify the IFT-B complex, and IFT140 and TULP3 to mark the IFT-A complex.[14] Recruitment/localization of these markers was tracked across multiple replicates and quantified, highlighting the reproducibility of our approach, as shown in Fig.2A.

This allowed us to build a temporal map of the steps involved in G_0 entry and ciliogenesis as summarized in Fig. 2B.[13-15,21-23] These include: (1) completion of cytokinesis by ~2hr; (2) recruitment of ARL13B and TTBK2 to the basal body within ~3-4hr; (4) RAB34 containing ciliary vesicle recruitment to the centrosome at ~6hr, with its loss by ~10hr; (5) transition from the Golgi (GM130) as the microtubule organizing center (MTOC) at 7hr to the centrosome as the MTOC starting at ~9hr, and transition zone formation (marked by Cep290 and acetylated tubulin) at ~9hr; (6) IFT-B recruitment (marked by IFT88) and ciliation (marked by acetylated tubulin) at ~10-11hr; (8) TULP3 recruitment at ~11hr followed by IFT-A (IFT140) recruitment at ~13hr; (9) axonemogenesis occurring over a 4hr window from ~13-17hr; (10) GPCR entry into cilia at ~18hr-20hr. Note that some of these key signals, including RAB34 and TULP3, have transient localizations inside the primary cilia and/or basal body.[24,25] These findings highlight the value of using synchronized model systems to track temporal-spatial signaling, as such transient signaling events may be missed in other contexts. For example, this is the first evidence, to our knowledge, that IFT-B recruits to basal bodies *before* IFT-A and that cilia appear to need to be fully formed before GPCR entry. Together, such findings reveal details concerning the stages of ciliogenesis and lay the groundwork for probing how and when defects in specific components alter these processes.

We also mapped changes in other key compartments, including trans-Golgi (TGN38) and cis-Golgi (GM130) network reassembly (Fig.1D,E 2hr window). The Golgi dynamically reorganizes in relation to the centrosome and basal body over time. After cytokinesis, the Golgi (GM130) serves as the primary MTOC at around ~7hr. By ~9hr, the acetylated tubulin-positive microtubules no longer colocalize strongly at the Golgi and instead begin to colocalize with the centrosome. Between 13-15hr, the basal body and growing primary cilium colocalize with Golgi. By ~17hr (after axonemogenesis), the cilium has reduced incidence of Golgi colocalization (Fig.1D). Furthermore, we note that as cells transition from mitosis deeper into the G_0 program, the number and the intensity of TGN38-positive TGN compartments reduces over time (Fig.1E). Future work can be done to establish the functionality of these compartments in G_0 and how they respond to different stimuli.

To determine if STAMP can be applied to other cell lines, we repeated these studies using SV40 immortalized MEFs (Fig.S2). Although different cell types differ in drug sensitivities, cell doubling times, or extent of ciliation, we found that synchronization of MEFs at metaphase produced a ~40% yield, slightly higher than RPE cells (~30%). Staining of the same ciliary markers in both MEFs and RPEs revealed conservation of the order of events but different kinetics for ciliogenesis. MEFs attached to the fibronectin-coated coverslips/plate much faster than RPE cells, already flattening on the plate at 20min post-seeding, while RPE cells are still rounded and in early cytokinesis. Ciliation also occurred at earlier time points in MEFs (~7hr) compared to RPE cells (~12hr). Together, these data reflect the general applicability of this synchronization strategy to diverse cell lines, though highlighting the need for optimization to map kinetics.

Phosphoproteomics reveals transient phosphorylations at distinct time points from mitosis to G_0 entry.

The high degree of cell synchronization achieved with our protocol allowed us to identify and further analyze transient events that otherwise are undetectable in a more heterogeneous cell population. Transient changes in PTMs drive coordinated cellular functions, so we employed phosphoproteomics to monitor phosphorylations at each time point shown in Fig.2B. We simultaneously harvested samples for IF and phosphoproteomics by seeding a coverslip in the same 10cm plate used to harvest cells for phosphoproteomics. This allowed us to optimally correlate cellular changes to both transient and stable phosphorylations in RPE cells. We observed >7500 phosphorylation sites, including several double, even triple phosphorylations using TiO_2 enrichment and timsTOF HT mass spectrometry. We provide an example of how we analyzed phosphosignatures in Fig.3A, looking at 3 different phosphosites on the centriolar satellite protein PCM1 and their relative fold change in normalized intensity over time. PCM1[S93] is an example of a very stable phosphorylation. We identified several such phosphorylations that remained constant throughout the time course, suggesting that their role was for general cellular functions (*e.g*, proteostasis, metabolic adaptation). In contrast, others showed dynamic changes in relative abundance that temporally correlated with specific stages of G_0. PCM1[S861] is specifically phosphorylated only during mitosis, while [T877] is elevated in the 13-15hr window (axonemogenesis). For phosphosignatures of interest, we analyzed the motif and searched the literature to identify known functions. Though all three of these sites were reported in PhosphoSite Plus, their functions are unknown. Overall, homogeneous cell populations allowed us to track context-specific, transient phosphorylations even on low-abundance proteins, many of which were identified less frequently in other published phosphoproteomic screens.[26] Less than 10% of the phosphorylations that we identified to date have an annotated, known functionality based on PhosphoSitePlus, and many of the reported functions for the “known” sites are inadequately characterized.

We can apply our approach to track changes in phosphosignals of proteins throughout the cell over time. These changes typically correlated with cellular events observed with IF. For example, we identified context-specific ciliary protein phosphorylations that are normally undetectable using phosphoproteomics and IF of asynchronous cells. We identified phosphorylations of known regulators of ciliary vesicle traffic that spike right when RAB34 recruits to the basal body (~7-8hr, and again at ~18-20hr): RAB34 [S241, S244] and MYO5A [S1652]. These and many other instances show the internal consistency between when modifications to these proteins are occurring and when these proteins are known to function both in the literature and based on our timeline (Fig.2B). We also tracked phosphorylations for known mitotic regulators to see if their temporal phosphosignatures corresponded with our IF data. We traced PLK1 and CDK1 activity in driving nuclear pore complex (NPC) disassembly during mitosis[27,28] by hyper-phosphorylating specific nucleoporins such as NUP35, NUP153, NUP188, and AHCTF1. In Fig.3C, we provide a STRING plot of all the components of the NPC complex that were phosphorylated in our study. All the phosphorylations annotated in the plot occur specifically within the 0-0.5hr window, consistent with their mitotic function. The colors of the phosphorylations indicate the putative or known kinase that makes these phosphorylations. Note that NUPs shown in this STRIING plot that are unphosphorylated in this window typically either were phosphorylated in cytokinesis or their phosphosignatures

remained constant throughout the time course. Beyond NPC machinery, we also detect phosphorylations of Golgi fragmentation regulators in mitosis (e.g, GOLGA1[S767], GM130[S37], BET1[S48]), consistent with Golgi fragmentation and later reassembly during the G_0 transition, consistent with our IF data (Fig.1D). Note that known phosphorylation markers of other states of cell cycle were undetectable under these conditions, including but not limited to G_1 (RB1 at [S780/S795], and [S807/S811]), G_1/S transition (RB1 [S612/S672] and p27 [T187]), S phase (H3[S10]), and G_2 (Cdc25[S216]). These signals are normally very pervasive and easy to detect in standard phosphoproteomics of heterogeneously cycling cells, even in asynchronous ciliogenesis samples. This suggests that STAMP phosphoproteomics specifically tracked the transition of cells from mitosis to quiescence, consistent with the IF data in Fig.1.

STAMP phosphoproteomics was especially useful for temporal-spatial mapping of transient phosphosignatures to regulators of established signaling pathways. For example, we mapped temporal phosphorylations to key components of the mTOR and protein synthesis pathway and observed key hierarchical signaling. In Fig.3D, we show the detailed map of the known components of the mTOR pathway and the signaling cascade by which they mediate critical cell functions, including translation and autophagy. We map onto this established pathway all the phosphorylations that we annotated via STAMP phosphoproteomics (colored rectangles), as well as the time frames in which these phosphorylations peaked in abundance (time windows marked in pink). The color of the phosphorylation shown indicates either the known (based on the literature) or putative kinases (as predicted based on the Cantley prediction algorithm[29]) that mediate these functions. The temporal mapping of phosphorylations of known function in the mTOR pathway proved especially valuable for identifying context-specific differential signaling. For example, GSK3β is a negative regulator of the mTOR pathway. Previous studies identified that GSK3β is activated by autophosphorylation at [Y216].[30] This ON signal is present throughout the time course, which would suggest at first glance that this kinase is always active and therefore mTOR signaling is OFF. With the power of temporal phosphoproteomics, though, we identify transient suppression of GSK3β by AKT and P38-induced phosphorylations ([S9] and [S389] respectively)[31,32] during the 0-3 and 6-12 hr windows. Therefore, because GSK3β suppression of mTOR is suppressed, this would suggest that mTOR signaling is ON but specifically only during mitosis through cytokinesis and during ciliogenesis licensing. This temporal mapping of phosphorylations allows us to resolve time and context-specific functions that would have been impossible to detect without STAMP. Exploration of signaling pathways and their dynamic functions throughout G_0 transition and in response to stimuli would be a rich field for future investigation.

Having identified strong correlations between phosphoproteomics and IF (Fig.2B), we applied this framework to generate hypotheses about the dynamics of the general cell program during the G_0 transition. We performed correlative analysis of all the temporal phosphosignatures to identify those with similar patterns and binned them to identify what cellular compartments/functions are undergoing changes in different time windows. In brief, data from 7 biological replicates (each with 3 technical replicates) were analyzed to identify trends in their temporal phosphosignatures. Phosphopeptides were sorted into 30 different groups and plotted in a heat map (Fig.3B). Each individual row of the map corresponds to a single phosphosignature and its change in relative abundance over time, with the x-axis on the bottom indicating the time and stage of ciliogenesis (based on IF).

Level of abundance is represented as a gradient of blue to yellow, with yellow being the highest abundance. The left of the map indicates the cluster numbers in which we binned phosphopeptides that shared the same temporal signatures of fluctuations in abundance (Fig.3B). In this way, we can look at the data from multiple angles, whether 1) finding a protein of interest, identifying the cluster(s) its phosphopeptides are in, and identifying putative functions, or 2) analyzing any individual cluster of interest to gauge what cell functions are acting in concert in each time frame during G_0 transition. In the latter case, we performed gene ontology (EnrichR) (Fig.S3) and Cytoscape analyses of individual clusters to identify trends in types of proteins undergoing phosphorylations at different time points (Fig.S3). These data were used to generate a temporal-spatial map of the phosphosignatures emerging through G_0 transition and linked to specific cellular locations or processes. Many of the functions identified via gene ontology occurred within the predicted time frame, based on our temporal-spatial mapping via IF (e.g, mitosis machinery in 0-0.5hr, endosome traffic 8hr and 12-20hr). We also identified trends that were indicative of novel functional windows. For example, we noted a class of phosphorylations that only emerged after cilia had fully formed (*i.e*, were at full length and had GPCRs inside), increasing at ~20hr and remaining elevated. These include CEP170[S1198], CCP110[S372], and CEP97[S114]. Note that CCP110 has known functions in preventing spurious ciliogenesis, but no function was reported for these factors later in the G_0 program. Together, the combination of IF, phosphoproteomics, and known function mapping enables the generation of novel, testable hypotheses as to the dynamic landscape of metaphase through G_0 transition. In the sections below, we provide examples of how we tested some of these hypotheses generated from phosphoproteomics and IF.

Defining detailed temporal-spatial pathways driving ciliogenesis via live cell imaging

We increased the temporal-spatial resolution of our approach via live cell imaging, which provided us with the tools to better track transient changes in cellular morphology and protein localization. As proof of principle, we performed STAMP synchronization using RPE cells stably expressing RABL2-GFP, a marker of distal appendages, and IFT88-mCherry, to mark IFT-B trains. We added SiR-tubulin to track axonemogenesis. We then performed multi-field, z-stack confocal imaging at 40x magnification, every 8 minutes over a 24hr time course. This revealed that essentially all cells began ciliogenesis within a 2hr window, starting at 11hrs (Fig.4C). Live cell imaging of synchronized cells also allowed us to determine the duration of specific cellular events on a cell-to-cell basis. For example, even though axonemogenesis in any given cell takes ~90min to complete,[15] axonemogenesis across the cell population occurred within a 3hr window (14-17hr; Fig.4C).

We also tracked the dynamic localization of the centrosome during different stages of the G_0 program (Fig.4E). After cells adhered to the plate, centrosomes localized basally. By 9 hrs 15 min after plating, the primary cilium had translocated to the apical cell surface.[33] This is about when the transition zone is being formed. After the cilium has formed and nearly completed importing receptors (~19hr), the basal body and its attached primary cilium sink basolaterally, usually to the side of the nucleus. We also posited that live cell imaging with STAMP provides a valuable approach for studying ciliary signaling. We stimulated the Sonic Hedgehog pathway with SAG (a synthetic Smoothened agonist, 200nM), and within 8 minutes of stimulation we observed basal to apical

translocation of primary cilia and increased accumulation of IFT88-mCherry particles at the basal body (Fig.4B). Thus, we can identify novel changes in the cell related to cilia and ciliary function and later employ MS and fixed cell imaging at specific time points to pursue mechanistic insights.

Though our initial focus was on ciliogenesis as a marker of quiescence transition, live cell imaging also provided insight into other aspects of cellular function. Within minutes after seeding, cells proceeded to cytokinesis, which finished within 2-3 hrs (Fig.4A). Interestingly, at ~2hrs, a short-lived phenomenon occurred in which tubulin accumulated at centrosomes, forming a “barrel-like” structure. These tubulin-rich barrels were encircled by IFT88 vesicles (Fig.4A). Less than an hour after forming, this tubulin structure dissipates, and the IFT88-positive vesicles become evenly distributed throughout the cell. Later (12hr), IFT88 positive vesicles aggregate around the centrosome (Fig.4D), with no sign of the return of the tubulin barrel intermediate. IFT88 later extends up the length of the growing cilium, consistent with IFT-B complex entry. Thus, the high degree of cell synchronization revealed a novel, currently unexplained, transient phenomenon of tubulin and IFT88 aggregation at centrosomes and allowed temporal resolution of key events.

Applying PIT-STAMP to dissect temporal-spatial mechanisms.

We predicted that cell synchronization would decrease background “noise” and would allow us to dissect the effects of individual regulators on different features of G_0 progression. To do so, we developed an approach called Pulsed Inhibitor Treatment (PIT)-STAMP, which involves the treatment of synchronized RPE cells at different times to determine the acute effects of loss of key regulators on the G_0 program. We began by using PIT-STAMP to test the hypothesis that translational control helps establish the G_0 program and ciliogenesis. Phosphoproteomics and Gene Ontology revealed phosphorylations of transcription and translation machinery at different stages of G_0 transition (Fig.3C,D, Fig.S3). Examples of such machinery include RSK2[S369], PRAS40 [T246], p70S6K [S447], NCL[S67], GAPDH[T177], YTHDF1[T202, S217], FXR2 [S601, S603], SSB [S92, S225], and LARP4B[S736, T732]- all of which peak at intensity at 4hr. RSK2[S369], in particular, is known for activating its function in transcriptional and translational control downstream of ERK.[34]

We then added the protein synthesis inhibitor cycloheximide (10µg/mL) for 1hr-long intervals starting at 4hr, 6hr, 10hr, and 16hr post-seeding. While ciliation was unchanged in cells treated with cycloheximide at the later time points, ciliogenesis was completely ablated in response to cycloheximide treatment at 4hr, even though the drug was removed at 5hr. This suggests that protein synthesis early in G_0 transition is essential for ciliogenesis. The role(s) of later windows of translational control in establishing the G_0 program is unknown but would be an exciting direction to study. When we looked again at mTOR pathway phosphorylations, key modifications peak at 4hr including known regulators of transcriptional and translational control. Altogether, these data establish a paradigm for future research into which proteins are synthesized in which G_0 transition windows and their respective functions.

PIT-STAMP also can be used to assess effects of inhibitors on regulators of specific pathways. We again use ciliogenesis as an example. We dosed cells with dynarrestin, a cytoplasmic dynein inhibitor that prevents microtubules association and, therefore, blocks retrograde ciliary transport.[35] We added dynarrestin (25µM) at

the same 1hr intervals described above for cycloheximide, followed by washout and fixation at 24hr (Fig.5A-C). Treatment with dynarrestin only inhibited ciliogenesis (from ~80% to ~5% ciliation) at the latest (16-17hr) window, or during axonemogenesis but before GPCR recruitment. A partial (~40% ciliation), though not significant, reduction of ciliogenesis occurred when added in the 10-11hr window. This is consistent with cytoplasmic dynein 1 and IFT being required to extend the axoneme and traffic key cargoes into growing cilia (Fig.5B-C).

Use of genetic modifications to aid in the ordering and dissection of specific processes.

We predicted that STAMP can also be used to dissect mechanisms of known but not fully characterized regulators of cell functions through performing the same procedures but in the context of genetic perturbation (*e.g*, CRISPR KO). To test this, we used STAMP to systematically phenotype ciliogenesis defects in ARL13B, TTBK2, and IFT52 KOs versus WT. Though each of these proteins are clearly important in ciliary function, the temporal-spatial mechanisms by which these factors drive ciliogenesis have yet to be elucidated.

Synchronization and IF of these three ciliogenesis defective cell lines revealed key differences concerning the nature of their ciliogenesis-defective lesions. Each of the three KO lines failed to ciliate (WT 80-90% versus ~0%; Fig.6A). However, the three KO lines diverged from each other in acetylated tubulin recruitment to the basal body and RAB34-positive ciliary vesicle recruitment. RAB34 recruitment in WT RPE occurs in two windows: peaking at ~7.5hr and again at ~20hr. TTBK2 KO cells recruited a first wave of RAB34 positive vesicles to the basal body (Fig. 6A). However, the second wave of RAB34 recruitment and GPR161 recruitment is lost in TTBK2 KOs. IFT52 KO showed both a reduced and delayed first wave of RAB34 recruitment, peaking at only ~40% of basal bodies positive for RAB34 (10hr), suggesting an earlier function in licensing (Fig.6A). As observed in the TTBK2 KOs, IFT52 KOs do not have a second wave of RAB34 recruitment but still have comparable acetylated tubulin recruitment to the basal body with WT. IFT52 KO cells show reduced GPR161 recruitment to basal bodies and defective intraflagellar traffic. In ARL13B KO cells, the first wave of RAB34 recruitment to the basal body is similar to WT, peaking at ~80% of cells at ~7.5hr, but there was no second wave. Instead, we observed a striking accumulation of RAB34 vesicles into what appears to be “aggregates" throughout the cell that began at 4hr and continued to enlarge throughout the rest of the time course (Fig.6B). ARL13B KOs also had defective acetylated tubulin recruitment, presenting with normal acetylated tubulin recruitment at 7.5hr which later dissipated at 10hr, with only ~20% of basal bodies being positive for acetylated tubulin by the end of the time course. Thus, the initial wave of ciliary vesicle recruitment is independent of TTBK2 but dependent/interconnected with ARL13B and IFT52/IFT-B function. Also, RAB34 plays a role in licensing acetylated tubulin recruitment and eventual extension of the axoneme. The degree to which each of these proteins is directly or indirectly involved in the function of these markers is currently unclear, but STAMP provides an optimized approach for future work pursuing mechanistic details. Altogether, STAMP combined with genetic manipulations serves as a powerful tool for dissecting the underlying mechanisms by which proteins regulate cellular processes and provides testable hypotheses for future studies.

Using STAMP to identify novel regulators of cellular functions in G_0

Based on the phosphoproteomics and correlative clustering that we performed above (Fig.3B), we hypothesized that novel regulators functioning in specific stages of ciliogenesis would share similar phosphosignature fluctuation patterns with known regulators of that function. We already identified known regulators of ciliogenesis and G_0 that exhibited phosphosignature patterns that correlated with the timing of their known functions and localization via IF, based on our ciliogenesis timeline (Fig.2B). Of the ~15,000 phosphorylations detected during the time course, ~7500 phosphosites showed dramatic changes in intensity that we later binned based on correlation analysis of phosphosignature patterning. Here we provide two examples of novel regulators identified from these analyses. Protein Kinase D1 (PRKD1) (Fig.6C) and Synaptic Vesicle Glycoprotein 2A (SV2A) (Fig.6D). PRKD1, which regulates TGN signaling,[36] revealed transient phosphosignatures that suggested activity during ciliogenesis/G_0. Multiple transient phosphosignatures were found for PRKD1, including [S249] which was elevated during cell division but decreased and completely disappeared over time. In contrast, phosphorylations on PRKD1[S397, T400] were seen only during vesicle recruitment and GPCR traffic windows (~6 and ~17hr windows; Fig.6C). We observed that PRKD1 also localizes to the basal body in two waves: in the 5-10hr and 17-20hr windows, consistent with it acting during vesicle recruitment and IFT and with phosphorylations being linked at least in time to the changes in localization.

We provide yet another proof of principle for STAMP as a tool for identifying novel regulators in the case of SV2A, an 83kDa transmembrane protein and galactose transporter that regulates neurotransmitter release.[37-39] The temporal phosphosignatures of SV2A were very similar to those of PCM1, a regulator of ciliogenesis that coordinates centriolar satellite remodeling to allow ciliation and is also critical for ciliary vesicle docking.[40-43] Specifically, SV2A is triply phosphorylated on S80, S81, and T84, resembling PCM1 phosphopeptides, including PCM1[S65, S68, S69]; and PCM1[S1765, S1768, S1776] (Fig.6D). These triple phosphorylations contain similar motifs suggestive of potential activation by the same kinase, likely through priming kinase activity (or a hierarchy of phosphorylations in which the first phosphorylation serves as a recognition motif for following phosphorylations). Based on these correlations, we predict that SV2A plays a role in vesicle recruitment to cilia. To test this hypothesis, we tracked SV2A distribution temporally in synchronized RPE cells (Fig.6D). We observed transient localization of SV2A to the basal body between 5-11hr and at what appears to be the transition zone of primary cilia at 17-18.5hr (Fig.6D). These time windows correspond with RAB34-positive vesicle recruitment windows, based on our temporal-spatial map (Fig.2). If SV2A is playing a direct role in ciliary vesicle traffic to drive ciliogenesis, we predicted that inhibition of SV2A would inhibit ciliogenesis specifically at stages associated with vesicle traffic. Therefore, we blocked SV2A activity using the highly selective SV2A inhibitor/ antiepileptic drug levetiracetam (50µg/mL) during 3 different time windows without washout (Fig.5A,D). Levetiracetam blocked ciliogenesis when added at 5hr, preventing effective TTBK2 recruitment and localization of acetylated tubulin, yet did not affect either IFTA/B recruitment or axonemogenesis. Interestingly, SV2A inhibition prevented GPR161 from entering primary cilia when added at 17 hr, consistent with roles for SV2A in coordinating ciliary traffic (Fig.5D). Altogether, STAMP provides us with the optimal system needed to explore both known and novel temporal-spatial mechanisms, setting the stage for more detailed network mapping of the G_0 program and other biological questions.

DISCUSSION

This study introduces STAMP, a new methodology that employs the power of imaging and phosphoproteomics in a synchronized cell population to identify and dissect detailed changes in cellular PTMs, localization, and function in time and space. We describe and give examples of just some of the many uses that STAMP can be used to determine sequence of events in multi-step processes (such as ciliogenesis or transition to G_0). By analyzing cells at different time points after release from mitosis, strong, testable hypotheses emerge. Our stringent G_0 entry synchronization protocol enables the enrichment and detection (in many cases for the first time) of rare, transient cellular events and PTMs of low abundant proteins. Note that while we focused herein on phosphorylations, other PTMs may be studied using the same protocols. We describe several applications that have already yielded new, exciting directions, though there are clearly many more potential uses for STAMP.

In establishing the timeline using live and fixed cell imaging (Fig.2B), we identified novel features to G_0 and ciliogenesis, including but not limited to (1) a novel “tubulin barrel” intermediate step at 2-3hr, (2) a hierarchy of recruitment in which IFT-B precedes IFT-A to the basal body, and (3) the discovery that ARL13B is recruited to basal bodies before TTBK2. Each of these observations opens up opportunities for discovery of molecular mechanisms. We also demonstrate the use of STAMP to analyze cells deleted for specific components of known pathways (ARL13B, IFT52, and TTBK2) to address and uncover ordering and mechanisms. We also give examples in which clustering of phosphosignatures, live cell imaging, and chemical inhibitors (PIT-STAMP) can be implemented to generate and begin to test novel hypotheses. For example, we identified new ciliogenesis regulators (featured here, PRKD1 and SV2A (Fig.5-6)), and a novel role for translational control in establishing quiescence. Furthermore, we temporally mapped known and novel phosphorylations to key regulators of mitosis (Fig.3C) and to mTOR pathway. Altogether, these findings solidify STAMP as a means of generating and testing hypotheses concerning the mechanisms driving essential life processes.

Overall, we believe the STAMP method has demonstrated the value of multiplexed studies to provide a more powerful approach to address cell regulation mechanisms. We pioneered an approach that resolves temporally coordinated, transient phosphorylations and cellular events via phosphoproteomics and microscopy, overcoming the typical background signal from cell cycle timing that has previously hindered such studies. This is important for dissecting higher-order signaling, or how different processes may be connected in time, space, and mechanism. Other techniques/tools can be multiplexed with STAMP, e.g., phosphosite-specific mutagenesis, RNA-seq, electron and super-resolution microscopy, other PTMs, other drug screens. Furthermore, our use of STAMP in MEFs supports our conclusion that this approach can be modified for use in a wide range of cell types, including cancerous cell lines. With STAMP, the ability to map signaling networks that drive biology and to ascertain how lesions in specific mechanisms propagate systemic cellular defects and disease will open doors not only for biology, but also for targeted therapeutic development.

ACKNOWLEDGEMENTS: RET was supported by Stanford Dean's Fellowship, NIH F32 1F32GM142180-01A1, and 1 K99 GM154060-01. PKJ was supported by NIH grants 5R01GM114276, 2TR01GM121565, and 5UL1TR00108502. This work was made possible by the Stanford Cell Sciences Imaging Facility. We would like

to extend special thanks to Tomoharu Kanie from UOHSC and Richard Kahn from Emory University for their critical feedback and input, as well as to Israel Larios and Roy Ng for providing instrumental technical support throughout the detailed experimental procedures.

AUTHOR CONTRIBUTIONS: Conceptualization- MOA, RET, and PKJ; Methodology- MOA, RET, LAX; Software, MOA, RET, LAX; Investigation- MOA, RET, LAX; Resources- PKJ; Writing- MOA, RET, PKJ; Supervision- PKJ; Funding Acquisition- RET, PKJ

DECLARATION OF INTERESTS:

The authors declare no competing interests.

FIGURE TITLES AND LEGENDS

Fig.1: *Rationale for the development of STAMP to dissect cell signaling*. (A) Schematic representing the various applications for synchronized cell populations, summarizing our approach for STAMP as a way of deciphering temporal-spatial mechanisms via live and fixed cell imaging as well as detailed mass spectrometry (in this case, proteomics and phosphoproteomics). Schematics were generated via BioRender. (B-D) Quantification of mitotic indices, Golgi morphology, Golgi versus centrosomal MTOC formation, and ciliation rate in STAMP-synchronized versus serum starved only cell populations, based on IF. These experiments were performed in biological replicate, n=100 per replicate. Error bars indicate SEM. (E) Example IF images of cells that were binned based on ciliation, Golgi morphology, MTOCs, or mitotic indices. For the 2hr timepoint, cells were stained for DAPI (blue), TGN38 (yellow), GM130 (cyan), and acetylated tubulin (magenta). For the 16hr time point, markers used were DAPI (blue) to mark nuclei, acetylated tubulin (white) to mark mitotic microtubules and primary cilia, and CEP170 to mark the basal body and midbody. Images were collected using widefield microscopy, 60x magnification, z-projection. Scale bars= 20μm.

Fig.2: *Developing a temporal-spatial map of quiescence via fixed cell imaging*. (A) Temporal-spatial map of the stages of exit from mitosis and cytokinesis and entry into G_0, as marked by ciliogenesis. This map was based on cells plated in serum-free medium on fibronectin coated plates, collecting time points approximately every hour over a 24hr period. This map summarizes the findings from compiled IF and live cell imaging data, collected from over multiple iterations of the STAMP protocol. The results were highly reproducible, with the temporal localization of key markers being consistent (within a 1-2hr margin) between experimental runs. Representative immunofluorescence images of key stages of ciliogenesis are shown below the map (widefield microscopy, 60x magnification, z-projection). Markers for each of the images are labeled with the respective name and color of the IF marker used. (B) Quantification of different markers of cell cycle/ciliogenesis/key cellular compartment morphologies to establish the temporal-spatial landscape of G_0 entry. Experiments were performed in replicate

and quantified over a range of time points after plating onto fibronectin coated coverslips. N= 100 cells per replicate, error bars= SEM.

Fig.3: *Phosphoproteomics reveals key signatures reflective of dynamic changes in the cellular landscape during the transition into quiescence*. (A) Above, example plot of the intensity of 3 different phosphosites of PCM1 over time. Below, a chart indicating the phosphosite, its corresponding motif, putative kinases that are strong candidates for making that modification (based on Cantley in vitro kinase activity screen) and predicted function (B) Clustered heat map of the normalized intensity of phosphopeptides after STAMP, as a compilation of 7 separate experiments with multiple technical replicates per each experiment. The color gradient goes from low (dark blue) to high (yellow) as indications of fold change, as shown on the right. On the bottom left, colored boxes indicate individual clusters in which phosphopeptides were binned based on similarities in the pattern of the intensity/abundance of individual phosphopeptides at different time points after seeding, which we term their "phosphosignatures." This heatmap was generated using R programming software, performing correlation analysis to cluster phosphopeptides with similar phosphosignature patterns. The left shows the number identifier of each cluster, which can be used to go to the Excel sheets and identify which phosphopeptides are within your cluster of interest. The bottom axis shows the time window and the ciliogenesis stage that occurs in this window. (C) Schematic representing NPC complex and phosphorylation events happening during mitosis. The phosphorylation boxes are color-coded with known or putative kinases for each phosphorylation site (see Kinase Key below). (D) Key examples of the vast array of temporally regulated phosphorylations of known mTOR and protein synthesis pathway machinery, as identified via STAMP. Each phosphorylation is annotated with the time of its peak (pink) and known/putative kinase (color coding of the phosphorylation, with Kinase Key on the left). The schematic was generated via BioRender.

Fig.4: *Live cell imaging reveals novel intermediate states in cell morphology and signaling during transition into quiescence*. Live cell time lapse imaging of STAMP synchronized, fluorescently tagged (IFT88-mCherry, RABL2-LAP(GFP)) and SiR-tubulin stained RPE cells over a 24hr-long time course. Images were collected at 40x magnification with z-stacks every ~8min, multiple fields per experiment. These experiments were performed in multiple replicates, with representative images included. Key examples of events captured via time-lapse imaging include the following: (A) a post-mitotic tubulin barrel at ~2hr, (B) ciliary migration within minutes of SHH induction, (C) axonemogenesis within a ~1hr time frame, (D) IFT88-positive vesicle recruitment to the centrosome before entry into the cilium at ~12hr, (E) dynamic basal body localization throughout the time course. All scale bars, unless indicated otherwise, are 20µm.

Fig.5: *Mapping the regulatory kinases and phosphatases that drive the intracellular landscape of G_0 transition*. (A) Timeline mapping when individual drug treatments were performed for PIT-STAMP, as mapped onto ciliogenesis as described previously in Figure 2. Red windows indicate when cycloheximide and dynarrestin drug treatments were performed (1hr spike-ins before washout, followed by endpoint fixation at 24hr), while blue windows refer to time frames in which SV2A inhibitor (levetiracetam) was added (long-term drug treatments but

collecting intermediate time points in between each window to track intermediate steps). (B) Representative images showing the differential effects of cycloheximide (CHX) and dynarrestin treatments at different windows (4hr vs 16hr window treatment) compared to DMSO control. Images were collected via widefield at 20x magnification using ImageXpress software. Blue= DAPI, magenta = CEP170, yellow = acetylated tubulin. Scale bar = 5μm. C) Quantification of ciliation rate in dynarrestin and CHX PIT-STAMP treated cells versus DMSO control. All experiments were performed in replicate, counting 100 cells for each phenotype after IF. Error bars = SEM. Statistics performed via Two-Way ANOVA, with *= 0.05, **=0.01, ***=0.001, ****=0.00001. Plots were generated with GraphPad Prism Software. (D) Quantification of IF images of PIT-STAMP for SV2A inhibitor treatments. Different markers were quantified for different treatment windows: Window 1- TTBK2, mitotic indices; Window 2- IFT140, IFT88, ciliation; Window 3- GPR161, ciliation. Experiments were performed in replicate, N=100 cells per replicate. Grey box= Window 1, Yellow Box = Window 2, Red box= Window 3.

Fig.6: *Applications of STAMP to decipher novel functions and regulators of G_0* transition. (A) Quantification of IF markers to compare rates of ciliogenesis and G_0 entry between different KOs: ARL13B vs TTBK2 vs IFT52 KO. Experiments were performed in replicate, N = 100 cells per replicate. (B) Representative images of Rab34 vesicle morphology in WT versus ARL13B KO RPEs 24hr post-initiation of STAMP. Z-stacks were collected via widefield microscopy at 60x magnification. (C) Representative images, quantification of localization to cilia/centrosome, and key phosphosignatures of PRKD1, a novel regulator of ciliogenesis. Images were collected via widefield microscopy at 60x magnification, error bar= 20μm. Quantification was performed in replicate, N= 100 cells per replicate. Phosphosignature mapping was performed to measure normalized intensity of different phosphopeptides for multiple replicates. (D) Representative images, quantification of localization to cilia/centrosome, and phosphosignatures of key phosphorylations for SV2A, another novel regulator of ciliogenesis. Images were collected via widefield microscopy at 60x magnification, error bar= 20μm. Quantification was performed in replicate, N= 100 cells per replicate. Phosphosignature mapping was performed to measure normalized intensity of different phosphopeptides for multiple replicates. Note that SV2A inhibitor was used above in Fig.5 to determine whether it also played a direct role in ciliation.

Fig. S1 Workflow of the STAMP synchronization protocol. (A) RPE and MEF cells were seeded at low density and were exposed to multiple different rounds of synchronization procedures before being harvested via mitotic shake-off. Schematic of the different stages captured by our synchronization protocol: metaphase onward through ciliogenesis and G_0 entry. (B) Quantification of ciliation of FBS-recovered versus non-FBS-recovered STAMP-synchronized cells as a control for synchronization protocol. Experiments were performed in replicate, N=100 per replicate. Error bars = SEM.

Fig. S2: Comparative STAMP of MEFs versus RPEs. Quantification of key markers of ciliogenesis/G_0 entry in RPEs versus MEFs via IF, including (A) mitotic indices, (B) ciliation, (C) acetylated tubulin at basal body, and (D) TTBK2 recruitment. Experiments were performed in replicate, N=100 per replicate. Error bars= SEM.

Fig. S3: Gene Ontology Mapping. Schematic summarizing the Gene Ontology analysis via EnrichR (https://maayanlab.cloud/Enrichr/). Individual clusters generated via mass spectrometry and heat mapping (see Figure 3) were run through the software, compared with the GO Biological Process 2023 analysis, and plotted via Bar Graphs and Clustergram. The top 4-5 functions for each cluster were mapped to the timeline as an unbiased approach to observe what functions are active at different time periods during G_0 entry.

STAR METHODS:

- RESOURCE AVAILABILITY

Lead contact

Further information and requests for resources and reagents should be directed to and will be fulfilled by the Lead Contact, Peter Jackson (pjackson@stanford.edu).

Materials availability

All unique/stable reagents generated in this study are available from the Lead Contact with a completed Materials Transfer Agreement.

Data and code availability

The published article includes all datasets generated during this study.

KEY NOTES ABOUT THIS PROTOCOL:

-The primary objective for this protocol was for purity of cell population, not for efficiency. We wanted to ensure that the conclusions we draw from these mass spectrometry and imaging approaches are accurate and to remove the obscurity that comes with having cells in mixed stages of cell cycle. Overall, we have achieved 40% efficiency (*i.e*, if we plated 100 cells, only 40 of them would be synchronized in mitosis by the end of the time course and usable for future assays). Therefore, when planning your experiment, make sure to calculate how many cells you will need at the end and seed at least 5x more cells than you would require. The efficiency issue likely can be resolved with future optimization (i.e. adjusting the timing of Palbociclib treatment and release from G_1, optimizing drug treatment concentrations). For our purposes, though, we prioritized purity over efficiency to maximize clean, interpretable signals for mass spectrometry.

-In the future, it would be interesting to repeat these studies using other cell lines. For example, it would be interesting to see how signaling events driving ciliation in internal versus external ciliogenesis vary. Note, though, that the protocol should be optimized for that particular cell line as different cell lines have different dwell times in different stages of cell cycle.

-Though we have made great strides in increasing the homogeneity of the cell population, we have to raise the caveat that this is just one facet of cells that could lead to heterogeneity in ciliation rates. Even clonal populations of cells change with increasing passage number, acquiring spontaneous mutations. Therefore, any remaining heterogeneity we see in ciliogenesis timing is likely due to factors that we have not controlled here.

MATERIALS USED:

- Cell lines used: WT hTERT RPE-1 originally was obtained from ATCC (CAT) and WT Mouse Embryonic Fibroblast were originally obtained from ATCC (cat #: CRL-2991). All stable cell lines (*i.e*, knockouts, ones expressing fluorescent labels) used in this experiment were generated from the original WT RPEs obtained from ATCC.
- Maintenance medium: DMEM/F12 (Thermofisher; cat #: 12400024) buffered with Sodium Bicarbonate (Gibco; 25080-094) + 10% FBS (Gemini; cat #: 100-106) + GlutaMax (Life Technologies; cat #: 35050-079) + Pen-Strep (Pen-Strep-Glutamine 100x, Gibco; cat #: 10378016)
- Serum starvation medium: DMEM/F12 + GlutaMax + Pen-Strep
- Puromycin: (SIGMA-Aldrich; P9620)
- Blasticidin: (Corning; 30-100-RB)
- Palbociclib (dissolved in DMSO)- 2.5mg/mL stocks (Selleck-Chem; cat #: S4482)
- Nocodazole (dissolved in DMSO)- 5mg/mL stocks (Cayman; cat #: 13857)
- Phosphate Buffered Saline (made in house using standard lab protocols)
- Appropriate plateware for specific assays:
    - BioLite 6-well Multidish Cell Culture-treated surface: (Thermo Scientific; cat #: 120184)
    - BioLite 100mm Tissue Culture Dish: (Thermo Scientific; cat #130182)
    - Roller bottles InVitro PETG Roller Bottles - 4200cm^2: (Thermofisher; 12-565-532)
    - Glass-bottom 96-well plates, black plate with lid (0.17+/- 0.005mm): (Cellvis; P96-1.5H-N)
    - BioLite 60 mm dish Cell Culture-Treated Surface
- Immunofluorescence reagents:
    - Microscope coverglass, 12CIR-1.5 (Fisherbrand, 12-545-81)
    - VistaVision Microscope Slides, Histobond (75x25x1mm) (VWR; cat #: 16005-110)
    - SlowFade Gold antifade reagent (Invitrogen; cat #: S36936)
    - DAPI, 10mg/mL (Biotium; cat #: 40043)
    - Primary antibodies:
        - Acetylated tubulin: (mouse IgG2B; Santa Cruz; Cat #: SC-23950; 1:5000 of 200µg/mL stock)
        - Cep170: (mouse IgG1; Thermo Scientific; Cat #: 41-3200; 1:1000 of 0.5mg/mL stock)
        - TTBK2: (rabbit; Sigma; Cat #: HPA018113; 1:250 of 0.4mg/mL stock)
        - GPR161: (rabbit; Proteintech; Cat #: 13398-1-AP; 1:500 of 0.7mg/mL stock)

- IFT140: (rabbit; Proteintech; Cat #: 17460-1-AP; 1:1000 of 0.9mg/mL stock)
- IFT188: (mouse IgG1; Proteintech; Cat #: 60227-1-Ig; 1:1000 of 1.4mg/mL stock)
- Cep290: (rabbit; Abcam; Cat #: ab85728; 1:500 of 1mg/mL stock)
- PDGFRα: (rabbit; Cell Signaling; Cat #: 3174; 1:500 of stock (unknown concentration))
- TULP3: (1:250 of Rabbit polyclonal, made in house)[14]
- SV2A: (rabbit; Thermofisher; Cat #: PA5-52476; 1:250 of 0.08 mg/mL)
- PRKD1: (rabbit; Sigma-Aldrich; Cat #: HPA029834; 1:250 of stock (unknown concentration))
- Rab34: (mouse IgG2a; Santa Cruz; Cat #: sc-376710; 1:250 of 0.2mg/mL)
- PCM1: (rabbit; gift from Dr. Andreas Merdes;[44] 1:1,000,000 of stock)
- ARL13B: (mouse IgG1; Santa Cruz; Cat #: sc-515784; 1:1000 of 0.2mg/mL stock)
- ARL13B: (rabbit; Proteintech; Cat #: 17711-1-AP; 1:1000 of 0.9mg/ML)
- FOP: (mouse IgG2B; Abnova; Cat #: H00011116-M01; 1:1000 of 0.1mg/mL)
- GM130: (rabbit; Cell Signaling; Cat #: 12480T; 1:000 of stock (unknown concentration))
- TGN38: (mouse IgG1; BD Biosciences; Cat #: 610898; 1:1000 of 0.25mg/mL)

  - Secondary antibodies: Alexafluors from Invitrogen
    - Donkey-anti-Rabbit 488 (cat #: A-32790)
    - Donkey-anti-Rabbit 568 (cat #: A-10042)
    - Donkey-anti-Rabbit 647 (cat #: A-21447)
    - Goat-anti-mouse IgG1 488 (cat #: A-21121)
    - Goat-anti-mouse IgG1 568 (cat #: A-21124)
    - Goat-anti-mouse IgG1 647 (cat #: A-21240)
    - Goat-anti-mouse IgG2a 488 (cat #: A-21131)
    - Goat-anti-mouse IgG2a 568 (cat #: A-21134)
    - Goat-anti-mouse IgG2a 647 (cat #: A-21241)
    - Goat-anti-mouse IgG2b 488 (cat #: A-21141)
    - Goat-anti-mouse IgG2b 568 (cat #: A-21144)
    - Goat-anti-mouse IgG2b 647 (cat #: A-21242)
  - Paraformaldehyde 16% Solution EM grade 10X10 ML (Electron Microscopy Sciences; cat #: 100503-917)
  - Methanol (Fisher Scientific; cat #: A412-4)
  - Triton X-100 (Fisher Scientific; cat #: AC21568-2500)
  - NP-40 substitute (Roche Applied Sciences; cat #: 11754599001)
- Phosphoproteomics reagents

- Sodium deoxycholate (Sigma; cat #: D6750)
- 2-Chloroacetamide (Sigma; cat #: C0267)
- Potassium hydroxide (Sigma; cat #: P5958)
- Calcium chloride (Sigma; cat #: 793639)
- Trifluoroacetic acid (Fisher; cat. #: AAL06374AC)
- Isopropanol (Fisher; cat. #: A461-1)
- Acetic acid (Fisher; cat. no. A11350)
- Tris(hydroxymethyl)aminomethane hydrochloride (Tris-HCl; cat. No. AC228031000)
- LC/MS Grade (Optima TM; cat. #: W6-4)
- Formic acid, 99.5%, LC/MS Grade (Optima TM; cat. #: A117-50)
- Tris(2-carboxyethyl)phosphine hydrochloride (Thermo Fisher; cat. #: PG82080)
- PierceTM BCA Protein Assay Kit (cat. #: 23225)
- PierceTM Bovine Serum Albumin (BCA) Standard Pre-Diluted Set (cat #: 23208)
- PierceTM Quantitative Colorimetric Peptide Assay (cat # 23275)
- Ammonia solution, 25% wt/vol (Honeywell; cat. #: 44273)
- Acetonitrile LC/MS grade (Honeywell; cat. #: 14261-1L)
- Potassium dihydrogen phosphate (Merck; cat. #: 5438410100)
- Methanol LC/MS grade (Millipore Sigma; cat. #: 900688-1L)
- Trypsin/Lys-C Mix, Mass Spec Grade (Promega, cat. #: V5073)
- Empore C18 47 mm Extraction Disk (Empore, cat. #: 320907D)
- Halt™ Protease Inhibitor Cocktail, EDTA-Free (Thermo Scientific, cat. #: 78425)
- Halt™ Phosphatase Inhibitor Cocktail, EDTA-Free (Thermo Scientific, cat. #: 78428)
- Bruker PepSep C18 10cm packed 1.5 µm beads in 150 um I.D column (Bruker; cat. #: 1893483) attached to the ZDV Sprayer (I.D. 20 µm, cat. #: 1865710)

- Live cell imaging reagents
  - SiR Tubulin live cell imaging dye (Cytoskeleton, Inc.; cat #: CY-SC002)
  - Imaging medium (phenol-red free, supplemented with HEPES, serum free) (Thermofisher; cat #: 11039021)
  - HEPES, 1M (Gibco; cat #: 15630080)
  - MatTEK glass bottom plates (MatTEK; cat #: P35G-1.5-14-C)
  - IBIDI 8-well glass bottom chamber slides (IBIDI, Cat #: 80827)

- Drug inhibitor treatments
  - SV2A inhibitor (levetiracetam) (Millipore-Sigma; cat #: L8668-50MG)
  - Cycloheximide (Sigma-Aldrich; cat #: C7698-1G)
  - Dynarrestin (Sigma-Aldrich; cat #: SML2332-5MG)
  - Dimethyl sulfide (DMSO) anhydrous, ≥99.9% (Sigma-Aldrich; cat #:276855)

GENERATION AND MAINTENANCE OF STABLE CELL LINES:

hTERT RPE-1 cells (ATCC; Cat #: CRL4000), HEK-293T, as well as all stable cell lines generated from this mother population were grown in DMEM/F-12 (12400024, Thermo Fisher Scientific) supplemented with 10% FBS (100–106, Gemini), 1× GlutaMax (35050-079, Thermo Fisher Scientific) at 37°C in 5% CO2. To induce cilium formation, RPE cells were incubated in DMEM/F12 supplemented with 1×GlutaMax (serum-free media). Cell lines were authenticated via a short-tandem-repeat based test. Mycoplasma negativity was confirmed via DAPI staining for all immunofluorescence experiments, screening for mycoplasma of all cell lines at least every month. All cells were maintained below passage 15 to prevent phenotypic/genetic drift and were raised without antibiotics except for endpoint assays to prevent the propagation of contaminated stocks.

CRISPR KO cell lines were generated as previously described.[13]

Stable cell lines expressing fluorescently tagged constructs were generated using lentivirus, as previously described (CITE KANIE PAPERS). Lentivirus carrying either gene of interest was produced by co-transfecting 293T cells with 150 ng of pCMV-VSV-G, 350 ng of pCMV-dR8.2 dvpr, and 500 ng of lenti-viral transfer plasmids previously described along with 3µL of Fugene 6 (E2692, Promega) transfection reagent. Media was replaced 24 hr after transfection to omit transfection reagent, and virus was harvested at 48 hr post-transfection. Virus was then filtered with a 0.45 µm PVDF filter (SLHV013SL, Millipore) and mixed with 4-fold volume of fresh media containing 12.5µg/mL polybrene (TR-1003-G, Millipore). Following infection for 66 hr, cells were selected with either 10µg/mL puromycin (P9620, SIGMA-Aldrich) or 10µg/mL blasticidin (30-100-RB, Corning) for at least 10 days before subsequent analysis.

SYNCHRONY PROCEDURE:

1. RPE cells were either seeded at 10% confluence to grow up for 24 hours (allowing them to double) or seeded at 20% confluence and allowed to settle for 6hrs. Ensure that the cells are evenly dispersed over the plate and avoid having any clumps. Cells that clump together tend to be less responsive to cell synchrony treatment and increase the likelihood of contaminating your sample.

2. Aspirate medium and replace with maintenance medium supplemented with Palbociclib at a final concentration of 1µg/mL. Incubate for 18hr at 37˚C. This will arrest the cells in G1.

3. Aspirate medium and wash at least 1x with PBS. Add fresh maintenance medium and let cells release from G1 for 8hr.

4. Aspirate medium and replace with maintenance medium supplemented with nocodazole at a final concentration of 50ng/mL. Incubate at 37˚C for 12 hr.

5. At this point it is good to look at your cells to make sure that you have successfully synchronized the cells. If your synchrony worked, you should see several rounded-up cells floating in the medium or still attached to the plate. These rounded cells are blocked in mitosis at approximately metaphase. At this time there will also be some cells that are still flat and attached to the plate, hence why we only have a ~30% synchrony efficiency. At this point, it is pivotal to only harvest the cells in mitosis and to avoid collecting the adherent cells.

6. Perform mitotic shakeoff- firmly tap on the side of the plates to try to increase the number of mitotic rounded cells that have detached from the plate. Use pipettor to suck up the supernatant and use it to gently wash off the mitotic cells. DO NOT be too rigorous, and DO NOT scrape the bottom of the plate. This step is pivotal for ensuring the purity of your sample and to avoid out-of-sync cells.

7. Spin down cells at 2500rpm for 5 min and aspirate supernatant. Resuspend in 10mL PBS to wash away remaining nocodazole medium.

8. Spin down cells at 2500rpm for 5 min and aspirate supernatant. Resuspend in 10mL maintenance medium and incubate the cells for 20 minutes at 37°C, KEEPING THE CELLS IN THE CONICAL TUBE. This step is pivotal- we have found incubating the cells for a short period in maintenance medium before thrusting them into serum starvation and before plating the cells allows the cells to recover faster and ciliate faster. By thrusting the cells straight into serum starvation medium and plating the cells directly, we noticed that it increased the time for axonemogenesis to occur by 6-8hr. We suspect it has something to do with helping to replenish the soluble pool of tubulin, but at the end of the day we're not too sure.

9. Spin down the cells at 3000rpm for 5 min, aspirate supernatant and resuspend in serum starvation medium. Make sure that the cells are not clumpy and have no signs of contamination with adherent cells (adherent cells that accidentally got scraped off tend to look less round and symmetric compared to mitotic cells) using visual inspection with brightfield microscopy. If the cells are clumpy, make sure to pipet up and down. We also do the added precautionary step of passing through the cells through a single-cell filter to avoid clumps that could contaminate the sample. Count the cells, and aliquot into appropriate vessels depending upon the purpose of your synchronized cells. See below:

IMMUNOFLUORESCENCE PROCEDURE:

1. For immunofluorescence, I typically plate cells onto acid-washed, non-coated coverslips inside 35mm individual dishes. This allows me to harvest individual time points as needed. We are aiming for the cells to be 80-90% confluent when they have settled down and have undergone one round of mitosis. So, I would recommend plating the cells at 50-60% confluence to ensure that you have plenty of cells to make that first double. So, approximately 5-6x10^5 cells per 35mm plate, per time point. Make sure to add the cells dropwise to the plate that already has medium coating the coverslips (this is important- we found if we put the cells in an

empty plate without medium already there that it leads to cells getting clumpy/unevenly distributed), rocking back and forth to ensure that the cells are evenly distributed.

2. Place plates in the incubator at 37°C, making sure not to stack plates but to put each one separately down on the rack. This is to ensure that they all reach the same temperature at the same time, which is critical for microtubule dynamics… otherwise the cells will not be synchronized, therefore making the time points incomparable.

3. Collect time points, fixing cells and staining cells according to standard in-house protocols. I would recommend some of the following preliminary markers to ensure that you've mastered synchrony before you proceed further:

a. Acetylated tubulin- great marker of cilia that should appear in all ciliating genotypes (some markers like ARL13B don't show up in every cilium depending on the genotype). I would always recommend having an acetylated tubulin channel on your coverslip for all comparisons, if possible.

i. Another bonus is that acetylated tubulin also markers the midbody and other key features in mitosis, so this coupled with a nice DAPI/nuclear stain can help you also quality control check to make sure you really synchronized your cells.

b. Cep170, centrin, or gamma tubulin to mark the basal body- this will help give you some sort of framework to tell if certain ciliogenesis markers have recruited/disappeared.

c. Cep164 and TTBK2 as early markers of ciliogenesis

d. Cep290 for transition zone, and I've also had good experience with NPHP4.

e. RAB34 for vesicle recruitment

f. GPR161 and PDGFR-alpha to mark ciliary receptors.

g. IFT88 (IFT-B), IFT140 (IFT-A), and TULP3 to mark ciliary traffic machinery.

4. If you are doing mass spectrometry or any other experiment, I would highly recommend always coupling with the experiment some time points for IF to coordinate with your other experiment samples. If you are using 10cm plates like in mass spec, you could even place the coverslip in the 10cm plate. This is a great way for sampling to ensure that what you see in the actual cells translates to molecular readout. Be aware that some fixation methods don't last very well long-term (*e.g*, methanol) so for those you might want to start the IF protocol on the same day as fixation. Others like PFA last long-term.

PHOSPHOPROTEOMICS PROCEDURE:

Stock solutions were prepared for the experiments, including 1 M Tris-HCl (pH 8.5), 5M potassium hydroxide (KOH), 100 mM KH_2PO_4, and 2 M calcium chloride ($CaCl_2$). All stock solutions were stored at room temperature (RT; 20–25 °C) and remained stable for more than one year.

10cm plates of cells (4x10^6 metaphase synchronized cells, accounting for the cells doubling to 8x10^6 cells) were collected for each replicate for each time point and processed for phosphoproteomics.

SDC lysis buffer was formulated with 4% (wt/vol) SDC and 100 mM Tris-HCl (pH 8.5) and 1x Halt™ protease and phosphatase Inhibitor cocktail. It was crucial to prepare this buffer freshly as SDC crystallizes upon storage in solution.

Reduction/alkylation buffer was composed of 100 mM TCEP and 400 mM 2-chloroacetamide (CAM), with pH adjusted to 7–8 using KOH. The pH of the buffer was verified using a pH indicator strip. This buffer had to be prepared immediately before use to ensure the full activity of CAM, and any excess had to be safely discarded after use.

Trypsin buffer was prepared by combining 0.05% (vol/vol) AcOH and 2 mM CaCl2. This buffer was stored at −20°C and remained stable for more than one year. For reconstitution, a 1-mg of lyophilized trypsin/Lys C was resuspended in 1 ml of trypsin buffer (1 mg ml^{-1}). The enzymes were resuspended by vortexing and then centrifuged (1,000g for 1 min at RT). Phosphoproteomic loading buffer was formulated with 6% (vol/vol) TFA/80% (vol/vol) ACN. Phosphoproteomic enrichment buffer consisted of 48% (vol/vol) TFA and 8mM KH2PO4.

Wash buffer was prepared using 5% (vol/vol) TFA/60% (vol/vol) ISO. Elution buffer was prepared by adding 200 µl of ammonia solution (NH4OH) to 800µl of 40% (vol/vol) ACN.

The SDC lysis buffer was chilled to 4°C. A 300 µl volume of lysis buffer was added to the 1x10^6 cells to achieve a protein concentration of approximately 3 mg/mL. The lysates were immediately heat-treated for 5 min at 95°C to facilitate lysis and inactivate endogenous proteases and phosphatases. Then, the lysates were homogenized by sonication at 4°C. Disulfide bonds and carbamidomethylated cysteine residues were reduced by adding a 1:10 volume (30 µl) of reduction/alkylation buffer to the samples. Samples were incubated for 5 minutes at 45°C with shaking at 1,500rpm. After removing the samples from heat and allowing them to cool to room temperature (RT), Lys-C and trypsin enzymes were added at an enzyme-to-substrate ratio of 1:100 (wt/wt) and the samples were digested overnight at 37°C with shaking at 1,500 rpm. To each sample, 400µl of ISO was added and thoroughly mixed at 1,500 rpm for 30s. Proper mixing with ISO was ensured before proceeding to the addition of EP enrichment buffer to prevent precipitate formation. A 100µL volume of EP enrichment buffer was added to the samples and mixed thoroughly at 1,500 rpm for 30 seconds. The samples were carefully inspected for the presence of precipitate or cloudiness. If any precipitate was observed, the samples were cleared by centrifugation (2,000g for 15 minutes at RT). The supernatants were then carefully transferred to clean tubes before TiO2 beads were added. The TiO2 beads were resuspended in EP loading buffer at a concentration of 1mg/µL. An aliquot of 20 mg suspended beads was pipetted into each sample, then incubated at 40 °C with shaking at 2,000rpm for 5 min. The beads were pelleted by centrifugation (2,000g for 1 min at RT), and the non-phosphopeptide supernatant was discarded using a glass aspirator tip attached to a vacuum hose. To the samples, 1 mL of EP wash buffer was added. Incubation was done at RT with shaking (2,000rpm) for 30s. The beads were pelleted by centrifugation (2,000g for 1min at RT). The supernatant was then discarded. Washing was repeated four more times, and the same wash procedure was performed. After the final wash, the

beads were resuspended in 75µl of EP.

Homemade Stage-Tips were constructed using two C18 Empore disks, following established procedures. The fabricated Stage-Tips were subjected to a washing process, which involved two washes with 100µL of methanol, one wash with 100µL of 80% acetonitrile/0.1% acetic acid, and two washes with 100µL of 1% acetic acid. Enriched phosphopeptides were loaded onto the Stage-Tips in 100µL of 1% acetic acid. Subsequently, the Stage-Tips were washed three times with 100µL of 1% acetic acid to remove salts. Finally, the phosphopeptides were eluted from the Stage-Tips using two elution steps of 30µL each, with 80% acetonitrile/0.1% acetic acid as the elution buffer.

Liquid Chromatography Setup:

A nanoELute ultra-high-pressure nano-flow chromatography system was utilized and directly coupled online with a hybrid trapped ion mobility spectrometry—quadrupole time-of-flight mass spectrometer (timsTOF Pro, Bruker) employing a nano-electrospray ion source (CaptiveSpray, Bruker Daltonics).

Chromatographic Conditions:

The liquid chromatography was conducted at a constant temperature of 50°C, employing a reversed-phase column (PepSep column, 10 cm × 150 µm i.d., packed with 1.5 µm C18-coated porous silica beads, Bruker) connected to the 10 µm emitter (Bruker). The mobile phase consisted of two components: Mobile Phase A, comprising water with 0.1/2% formic acid/ACN (v/v), and Mobile Phase B, comprising ACN with 0.1% formic acid (v/v).

Gradient Elution:

During the 60-minute experiments, peptide separation was achieved using a linear gradient from 2-33% Mobile Phase B within 60 minutes. This was followed by a washing step with 95% Mobile Phase B and subsequent re-equilibration. The chromatographic process maintained the flow rate at 400nL/min.

Data Analysis:

Raw data files were processed using MS Fragger software against the NCBI Homo sapiens RefSeq protein database. Search parameters included CID fragmentation ion types with a precursor error tolerance of 20 ppm and a fragment ion tolerance of 40 ppm. Searches included S/T/Y phosphorylation and up to three modifications per peptide beside standard modifications. Peptides were validated using Percolator and Protein Prophet at 1% FDR. Protein quantification was performed using IonQuant, with normalization across runs and Match Between Runs settings accommodating retention time and ion mobility tolerances of 0.4 minutes and 0.05 (1/K0), respectively. Further analysis was performed, and manual validations were performed on the Skyline for the low-abundance phosphorylation-like ciliary ones.[45]

LIVE CELL IMAGING PROCEDURE

1. Precoat glass bottom, live cell imaging plates (Ibidi 8-well; Cat #: 80827) for 30 minutes at 37°C with fibronectin (Sigma; FC010-5MG) diluted in PBS (10µg/mL)
2. Plate cells at ~60% confluence directly into serum free imaging medium in live cell imaging plate (phenol red free DMEM/F12 + Glutmax, supplemented with HEPES), anticipating at least a doubling to get 100% confluence to ensure optimal conditions for inducing ciliogenesis. For the purposes of this study, we used cells stably expressing RABL2-GFP and IFT88-mCherry to visualize ciliogenesis. We incubated the cells with SiR-Tubulin live cell imaging dye (far red) at 1:500 dilution to visualize the formation of the axoneme. Different live cell imaging markers can be used to address different experimental questions using the same protocols.
3. Place cells on stage of live-cell imaging chamber-equipped confocal. We used an Inverted Zeiss LSM 880 Laser Scanning Confocal Microscope. Z-projections (10-12 slices each) were collected every 8 minutes from 4 different fields over a 24hr time course. These conditions can be optimized based on the question, including increasing number of time points, reducing the number of slices, focusing on specific time windows rather than the full ciliogenesis time course, etc.
4. TIPS FOR REDUCING PHOTOTOXICITY:
    a. Increasing the medium in the well helps to reduce the concentration of ROSs produced due to light exposure.
    b. Optimize the number of time points and z-stacks collected per well to increase information without risking damaging the cells. Depending on the nature of your question, you may want to prioritize cell health and endurance over detailed temporal/spatial information.
    c. Minimize laser power and gain. Data processing by adjusting the lookup tables can help with letting you see your data without risking cell damage.
    d. Live cell imaging medium supplemented with HEPES (to modulate pH) and that is phenol-red free (to reduce autofluorescence) helps reduce phototoxicity.

QUANTIFICATION AND STATISTICAL ANALYSIS

Unless otherwise stated, 100 cells were scored per each replicate, and all experiments were performed in at least triplicate and scored in at least duplicate. Data were processed using Excel and graphed using GraphPad Prism, and error bars shown indicate the SEM for the data set. Individual data points signify the average of technical replicates for each individual cell line. Statistical significance of the difference between individual test groups was assessed using either one-way or two-way ANOVAs: * = $p < 0.05$; ** = $p < 0.01$; *** = $p < 0.001$, **** = $p < 0.0001$.

REFERENCES:

1 Ardito, F., Giuliani, M., Perrone, D., Troiano, G. & Lo Muzio, L. The crucial role of protein phosphorylation in cell signaling and its use as targeted therapy (Review). *Int J Mol Med* **40**, 271-280 (2017). https://doi.org/10.3892/ijmm.2017.3036

2 Sanchez, I. & Dynlacht, B. D. Cilium assembly and disassembly. *Nat Cell Biol* **18**, 711-717 (2016). https://doi.org/10.1038/ncb3370

3 Reiter, J. F. & Leroux, M. R. Genes and molecular pathways underpinning ciliopathies. *Nat Rev Mol Cell Biol* **18**, 533-547 (2017). https://doi.org/10.1038/nrm.2017.60

4 Mill, P., Christensen, S. T. & Pedersen, L. B. Primary cilia as dynamic and diverse signalling hubs in development and disease. *Nat Rev Genet* **24**, 421-441 (2023). https://doi.org/10.1038/s41576-023-00587-9

5 May-Simera, H. L. *et al.* Primary Cilium-Mediated Retinal Pigment Epithelium Maturation Is Disrupted in Ciliopathy Patient Cells. *Cell Rep* **22**, 189-205 (2018). https://doi.org/10.1016/j.celrep.2017.12.038

6 Avasthi, P., Maser, R. L. & Tran, P. V. Primary Cilia in Cystic Kidney Disease. *Results Probl Cell Differ* **60**, 281-321 (2017). https://doi.org/10.1007/978-3-319-51436-9_11

7 Lee, E. Y. & Hughes, J. W. Rediscovering Primary Cilia in Pancreatic Islets. *Diabetes Metab J* **47**, 454-469 (2023). https://doi.org/10.4093/dmj.2022.0442

8 Hughes, J. W. *et al.* Primary cilia control glucose homeostasis via islet paracrine interactions. *Proc Natl Acad Sci U S A* **117**, 8912-8923 (2020). https://doi.org/10.1073/pnas.2001936117

9 Wu, C. T. *et al.* Discovery of ciliary G protein-coupled receptors regulating pancreatic islet insulin and glucagon secretion. *Genes Dev* **35**, 1243-1255 (2021). https://doi.org/10.1101/gad.348261.121

10 Hilgendorf, K. I. *et al.* Omega-3 Fatty Acids Activate Ciliary FFAR4 to Control Adipogenesis. *Cell* **179**, 1289-1305 e1221 (2019). https://doi.org/10.1016/j.cell.2019.11.005

11 Steger, M. *et al.* Systematic proteomic analysis of LRRK2-mediated Rab GTPase phosphorylation establishes a connection to ciliogenesis. *Elife* **6** (2017). https://doi.org/10.7554/eLife.31012

12 O'Toole, S. M. & Chapple, J. P. Primary cilia: a link between hormone signalling and endocrine-related cancers? *Biochem Soc Trans* **44**, 1227-1234 (2016). https://doi.org/10.1042/BST20160149

13 Kanie, T., Love, J. F., Fisher, S. D., Gustavsson, A. K. & Jackson, P. K. A hierarchical pathway for assembly of the distal appendages that organize primary cilia. *bioRxiv* (2023). https://doi.org/10.1101/2023.01.06.522944

14 Mukhopadhyay, S. *et al.* TULP3 bridges the IFT-A complex and membrane phosphoinositides to promote trafficking of G protein-coupled receptors into primary cilia. *Genes Dev* **24**, 2180-2193 (2010). https://doi.org/10.1101/gad.1966210

15 Westlake, C. J. *et al.* Primary cilia membrane assembly is initiated by Rab11 and transport protein particle II (TRAPPII) complex-dependent trafficking of Rabin8 to the centrosome. *Proc Natl Acad Sci U S A* **108**, 2759-2764 (2011). https://doi.org/10.1073/pnas.1018823108

16 Loktev, A. V. *et al.* A BBSome subunit links ciliogenesis, microtubule stability, and acetylation. *Dev Cell* **15**, 854-865 (2008). https://doi.org/10.1016/j.devcel.2008.11.001

17 Nachury, M. V. Tandem affinity purification of the BBSome, a critical regulator of Rab8 in ciliogenesis. *Methods Enzymol* **439**, 501-513 (2008). https://doi.org/10.1016/S0076-6879(07)00434-X

18 Nachury, M. V. *et al.* A core complex of BBS proteins cooperates with the GTPase Rab8 to promote ciliary membrane biogenesis. *Cell* **129**, 1201-1213 (2007). https://doi.org/10.1016/j.cell.2007.03.053

19 Hayman, E. G., Pierschbacher, M. D., Suzuki, S. & Ruoslahti, E. Vitronectin--a major cell attachment-promoting protein in fetal bovine serum. *Exp Cell Res* **160**, 245-258 (1985). https://doi.org/10.1016/0014-4827(85)90173-9

20 Hannan, G. N. & Reilly, W. Adsorption from fetal calf serum of collagen-like proteins which bind fibronectin and promote cell attachment. *Exp Cell Res* **178**, 343-357 (1988). https://doi.org/10.1016/0014-4827(88)90404-1

21 Goetz, S. C., Liem, K. F., Jr. & Anderson, K. V. The spinocerebellar ataxia-associated gene Tau tubulin kinase 2 controls the initiation of ciliogenesis. *Cell* **151**, 847-858 (2012). https://doi.org/10.1016/j.cell.2012.10.010

22 Laporte, M. H. *et al.* Time-series reconstruction of the molecular architecture of human centriole assembly. *Cell* **187**, 2158-2174 e2119 (2024). https://doi.org/10.1016/j.cell.2024.03.025

23 Mercey, O., Mukherjee, S., Guichard, P. & Hamel, V. The molecular architecture of the ciliary transition zones. *Curr Opin Cell Biol* **88**, 102361 (2024). https://doi.org/10.1016/j.ceb.2024.102361

24 Bruel, A. L. *et al.* Pathogenic RAB34 variants impair primary cilium assembly and cause a novel oral-facial-digital syndrome. *Hum Mol Genet* **32**, 2822-2831 (2023). https://doi.org/10.1093/hmg/ddad109

25 Ganga, A. K. *et al.* Rab34 GTPase mediates ciliary membrane formation in the intracellular ciliogenesis pathway. *Curr Biol* **31**, 2895-2905 e2897 (2021). https://doi.org/10.1016/j.cub.2021.04.075

26 Hornbeck, P. V. *et al.* 15 years of PhosphoSitePlus(R): integrating post-translationally modified sites, disease variants and isoforms. *Nucleic Acids Res* **47**, D433-D441 (2019). https://doi.org/10.1093/nar/gky1159

27 de Castro, I. J., Gil, R. S., Ligammari, L., Di Giacinto, M. L. & Vagnarelli, P. CDK1 and PLK1 coordinate the disassembly and reassembly of the nuclear envelope in vertebrate mitosis. *Oncotarget* **9**, 7763-7773 (2018). https://doi.org/10.18632/oncotarget.23666

28 Linder, M. I. *et al.* Mitotic Disassembly of Nuclear Pore Complexes Involves CDK1- and PLK1-Mediated Phosphorylation of Key Interconnecting Nucleoporins. *Dev Cell* **43**, 141-156 e147 (2017). https://doi.org/10.1016/j.devcel.2017.08.020

29 Johnson, J. L. *et al.* An atlas of substrate specificities for the human serine/threonine kinome. *Nature* **613**, 759-766 (2023). https://doi.org/10.1038/s41586-022-05575-3

30 Cole, A., Frame, S. & Cohen, P. Further evidence that the tyrosine phosphorylation of glycogen synthase kinase-3 (GSK3) in mammalian cells is an autophosphorylation event. *Biochem J* **377**, 249-255 (2004). https://doi.org/10.1042/BJ20031259

31 Thornton, T. M. *et al.* Phosphorylation by p38 MAPK as an alternative pathway for GSK3beta inactivation. *Science* **320**, 667-670 (2008). https://doi.org/10.1126/science.1156037

32 Salas, T. R. *et al.* Alleviating the suppression of glycogen synthase kinase-3beta by Akt leads to the phosphorylation of cAMP-response element-binding protein and its transactivation in intact cell nuclei. *J Biol Chem* **278**, 41338-41346 (2003). https://doi.org/10.1074/jbc.M302972200

33 Pitaval, A. *et al.* Microtubule stabilization drives 3D centrosome migration to initiate primary ciliogenesis. *J Cell Biol* **216**, 3713-3728 (2017). https://doi.org/10.1083/jcb.201610039

34 Yang, T. T., Xiong, Q., Graef, I. A., Crabtree, G. R. & Chow, C. W. Recruitment of the extracellular signal-regulated kinase/ribosomal S6 kinase signaling pathway to the NFATc4 transcription activation complex. *Mol Cell Biol* **25**, 907-920 (2005). https://doi.org/10.1128/MCB.25.3.907-920.2005

35 Hoing, S. *et al.* Dynarrestin, a Novel Inhibitor of Cytoplasmic Dynein. *Cell Chem Biol* **25**, 357-369 e356 (2018). https://doi.org/10.1016/j.chembiol.2017.12.014

36 Su, Y. *et al.* The protein kinase D1-mediated classical protein secretory pathway regulates the Ras oncogene-induced senescence response. *J Cell Sci* **131** (2018). https://doi.org/10.1242/jcs.207217

37 Bindra, P. S., Knowles, R. & Buckley, K. M. Conservation of the amino acid sequence of SV2, a transmembrane transporter in synaptic vesicles and endocrine cells. *Gene* **137**, 299-302 (1993). https://doi.org/10.1016/0378-1119(93)90024-w

38 Feany, M. B. & Buckley, K. M. The synaptic vesicle protein synaptotagmin promotes formation of filopodia in fibroblasts. *Nature* **364**, 537-540 (1993). https://doi.org/10.1038/364537a0

39 Wu, P. P., Cao, B. R., Tian, F. Y. & Gao, Z. B. Development of SV2A Ligands for Epilepsy Treatment: A Review of Levetiracetam, Brivaracetam, and Padsevonil. *Neurosci Bull* **40**, 594-608 (2024). https://doi.org/10.1007/s12264-023-01138-2

40 Hall, E. A. *et al.* Centriolar satellites expedite mother centriole remodeling to promote ciliogenesis. *Elife* **12** (2023). https://doi.org/10.7554/eLife.79299

41 Kubo, A., Sasaki, H., Yuba-Kubo, A., Tsukita, S. & Shiina, N. Centriolar satellites: molecular characterization, ATP-dependent movement toward centrioles and possible involvement in ciliogenesis. *J Cell Biol* **147**, 969-980 (1999). https://doi.org/10.1083/jcb.147.5.969

42 Ansley, S. J. *et al.* Basal body dysfunction is a likely cause of pleiotropic Bardet-Biedl syndrome. *Nature* **425**, 628-633 (2003). https://doi.org/10.1038/nature02030

43 Vladar, E. K. & Stearns, T. Molecular characterization of centriole assembly in ciliated epithelial cells. *J Cell Biol* **178**, 31-42 (2007). https://doi.org/10.1083/jcb.200703064

44 Dammermann, A. & Merdes, A. Assembly of centrosomal proteins and microtubule organization depends on PCM-1. *J Cell Biol* **159**, 255-266 (2002). https://doi.org/10.1083/jcb.200204023

45 Pino, L. K. *et al.* The Skyline ecosystem: Informatics for quantitative mass spectrometry proteomics. *Mass Spectrom Rev* **39**, 229-244 (2020). https://doi.org/10.1002/mas.21540

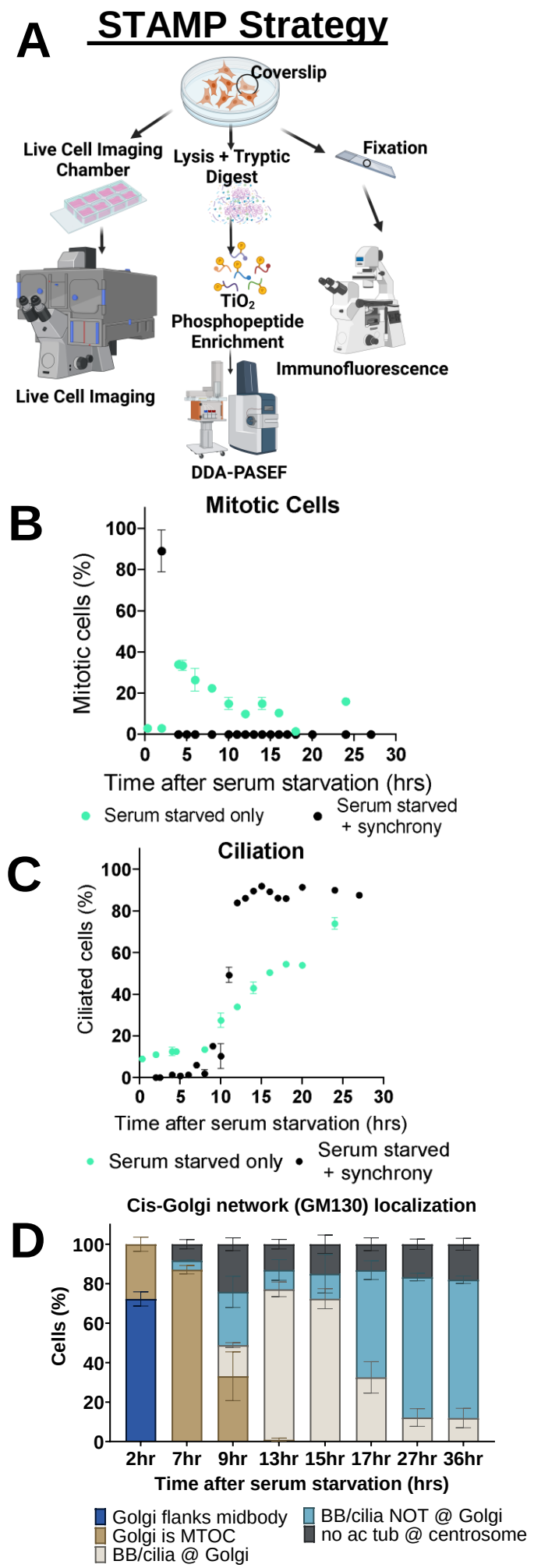
A
STAMP Strategy
Coverslip
Live Cell Imaging Chamber
Lysis + Tryptic Digest
Fixation
TiO2 Phosphopeptide Enrichment
Immunofluorescence
Live Cell Imaging
DDA-PASEF
B
Mitotic Cells
Mitotic cells (%)
Time after serum starvation (hrs)
Serum starved only
Serum starved + synchrony
C
Ciliation
Ciliated cells (%)
Time after serum starvation (hrs)
Serum starved only
Serum starved + synchrony
D
Cis-Golgi network (GM130) localization
Cells (%)
2hr 7hr 9hr 13hr 15hr 17hr 27hr 36hr
Time after serum starvation (hrs)
Golgi flanks midbody
Golgi is MTOC
BB/cilia @ Golgi
BB/cilia NOT @ Golgi
no ac tub @ centrosome

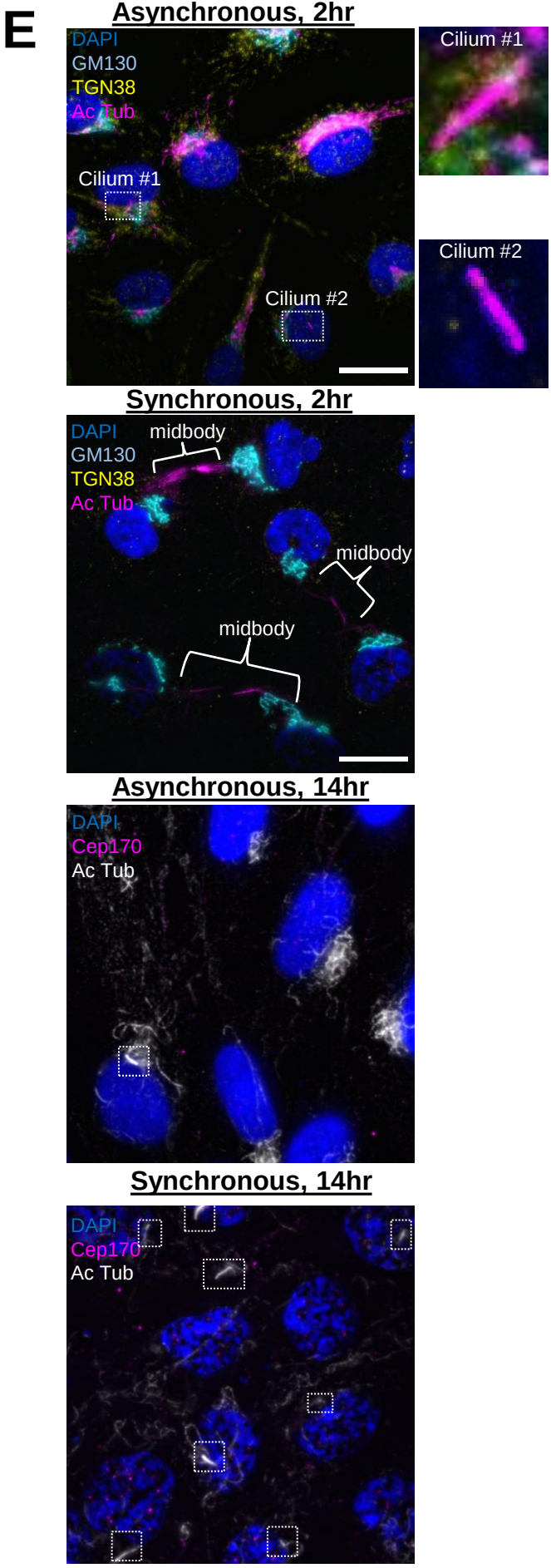
E
Asynchronous, 2hr
DAPI
GM130
TGN38
Ac Tub
Cilium #1
Cilium #2
Synchronous, 2hr
midbody
Asynchronous, 14hr
Cep170
Synchronous, 14hr

Figure 1

A

Quantitation of markers to map ciliogenesis in time

TTBK2 recruitment
Cells w/ TTBK2 to BB (%)
Time after serum starvation (hrs)

ARL13B localization
Cells (%)
Time after serum starvation (hrs)
Centrosomal • Ciliary

Acetylated tubulin at BB
Cells with ac tub at BB (%)
Time after serum starvation (hrs)

Axoneme length
Average ciliary length (μm²)
Time after serum starvation (hrs)

Cep290 at Transition Zone
Cells w/ Cep290 at BB (%)
Time after serum starvation (hrs)

RAB34 at BB
Cells w/ Rab34 at BB (%)
Time after serum starvation (hrs)

PCM1 localization
Cells (%)
Time after serum starvation (hrs)
dispersed
BB + rootlet
BB only
BB + ac tub/cilia

PDGRFα localization
Cells (%)
Time after serum starvation (hrs)
unciliated cells
inside cilia, diffuse
cilia, no PDGRFa
inside cilia, punct
cilia, base only

IFT88 localization
Cells (%)
Time after serum starvation (hrs)
unciliated cells
inside cilia, punctate
cilia, no IFT88
inside cilia, diffuse
cilia, base only

IFT140 localization
Cells (%)
Time after serum starvation (hrs)
Unciliated cells
inside cilia, punctate
cilia, no IFT140
inside cilia, diffuse
cilia, base only

TULP3 localization
Cells (%)
Time after serum starvation (hrs)
no cilia
inside cilia, punctate
ciliated, no TULP3
inside cilia, diffuse
ciliated, base only

GPR161 localization
Cells (%)
Time after serum starvation (hrs)
unciliated
inside cilia
cilia, no GPR161
cilia, at base

B

Temporal-spatial map of ciliogenesis

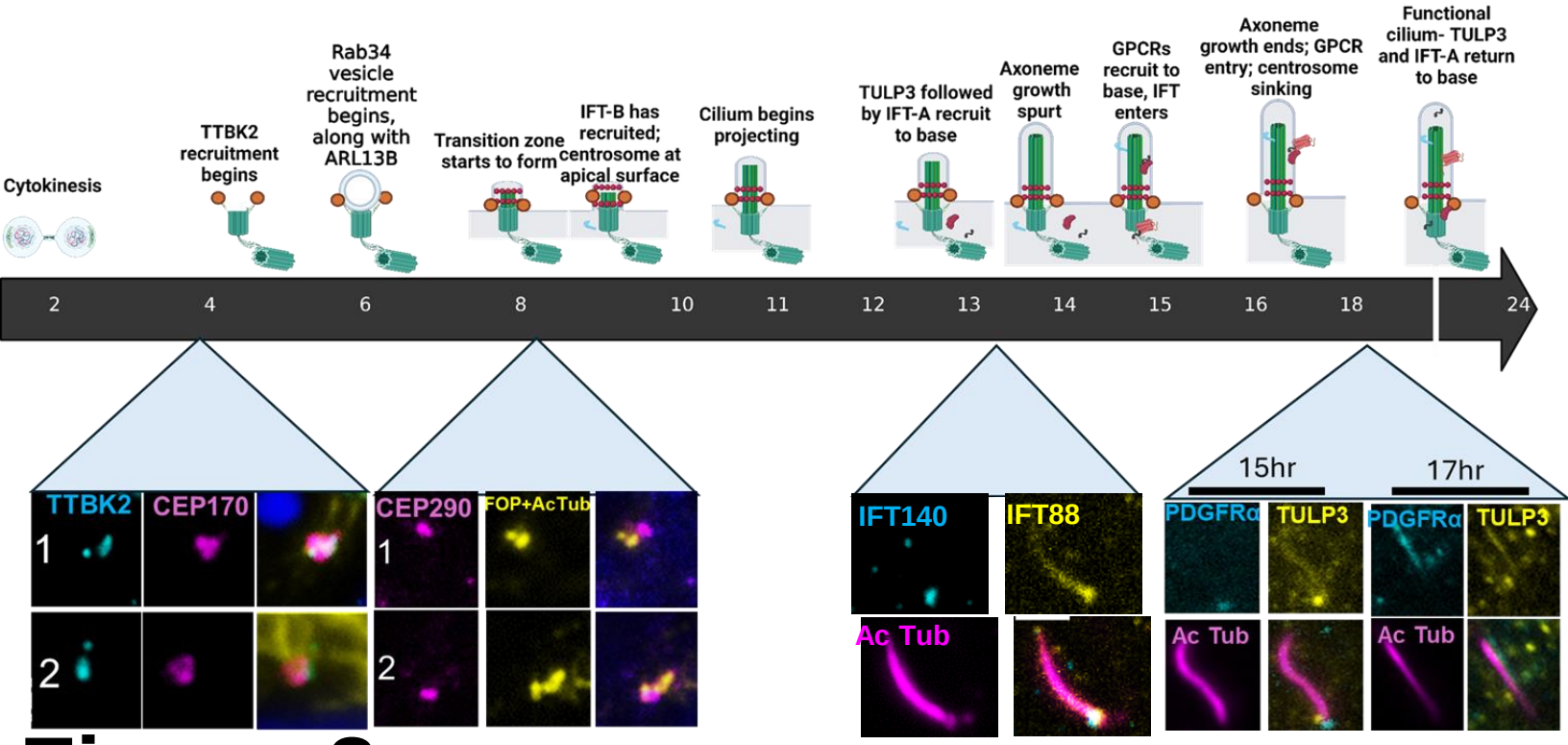

Figure 2

A

Example of interpreting phospho-signatures: **PCM1**

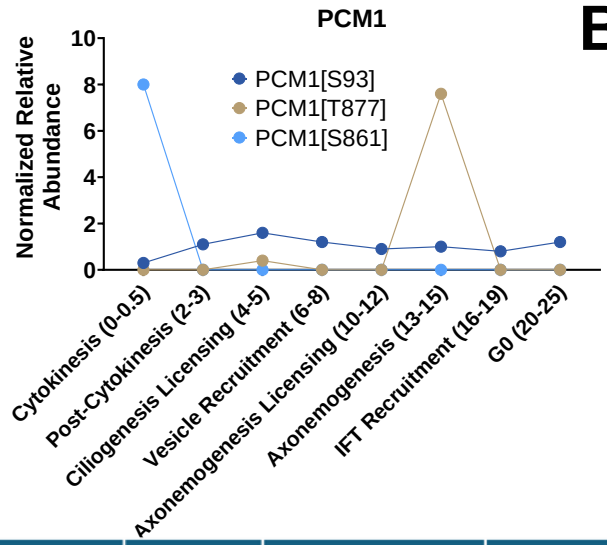

B

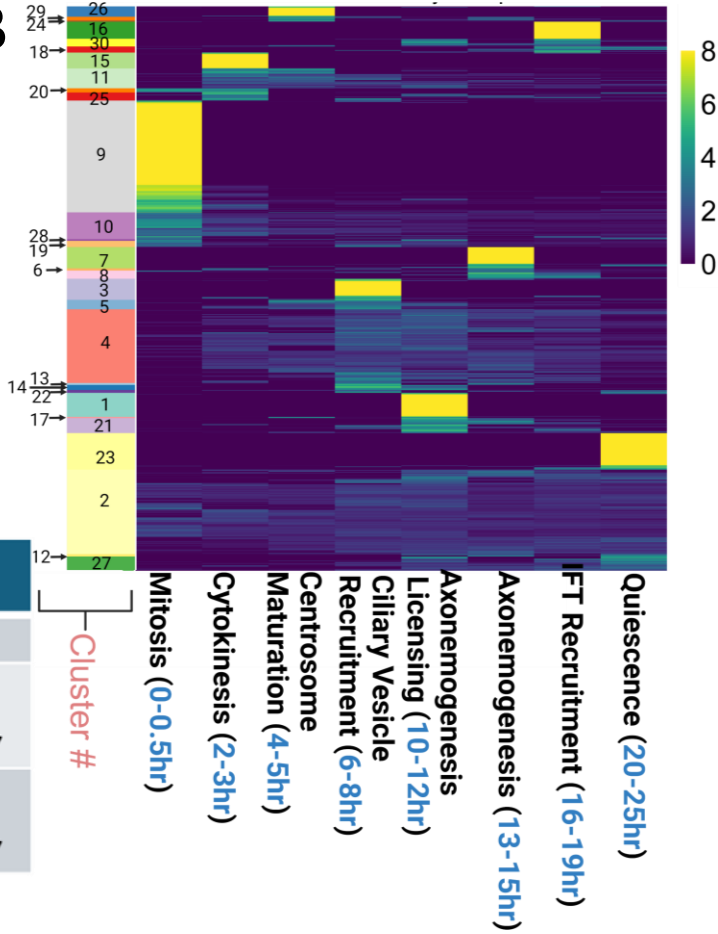

Site	Motif	Cluster	Predicted fxn	Putative Kinase
[S93]	**YMSQMsVPEQAE**	#2	Not G_0	MAPK
[T877]	**GSENLCtPQQSRT**	#7	Axonemogenesis	JNK1,2,3 P38D CDK16/17
[S861]	**QGLAETAsPVAVSLR**	#9	Mitosis	JNK1,2,3 P38D CDK16/17

C

NPC's Phosphorylations during Mitosis (0-0.5hr)

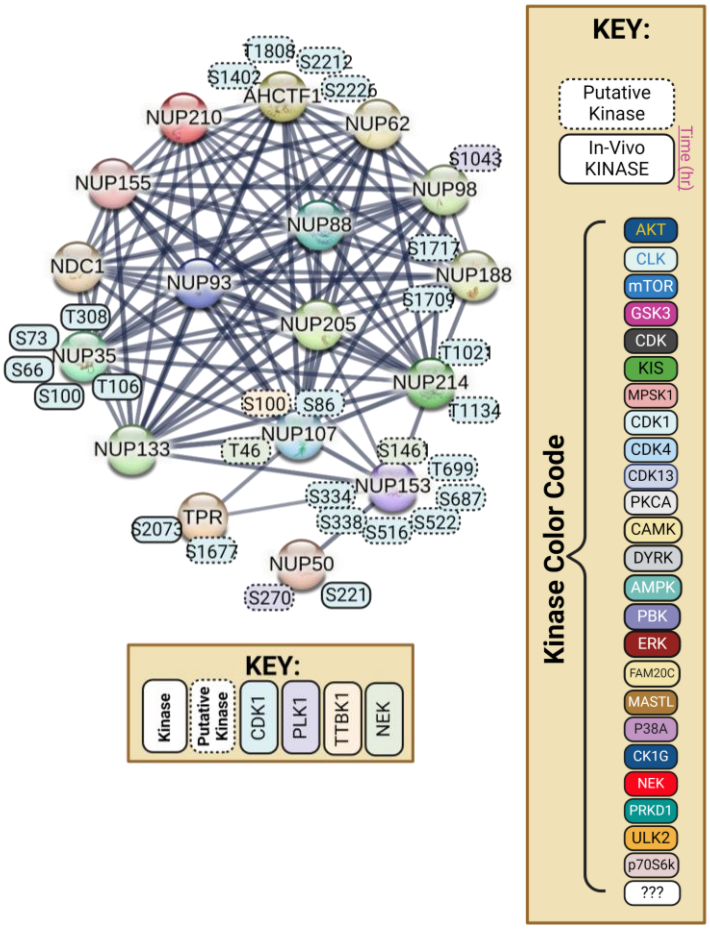

Temporal Mapping of mTOR Signaling Pathway Phosphorylations

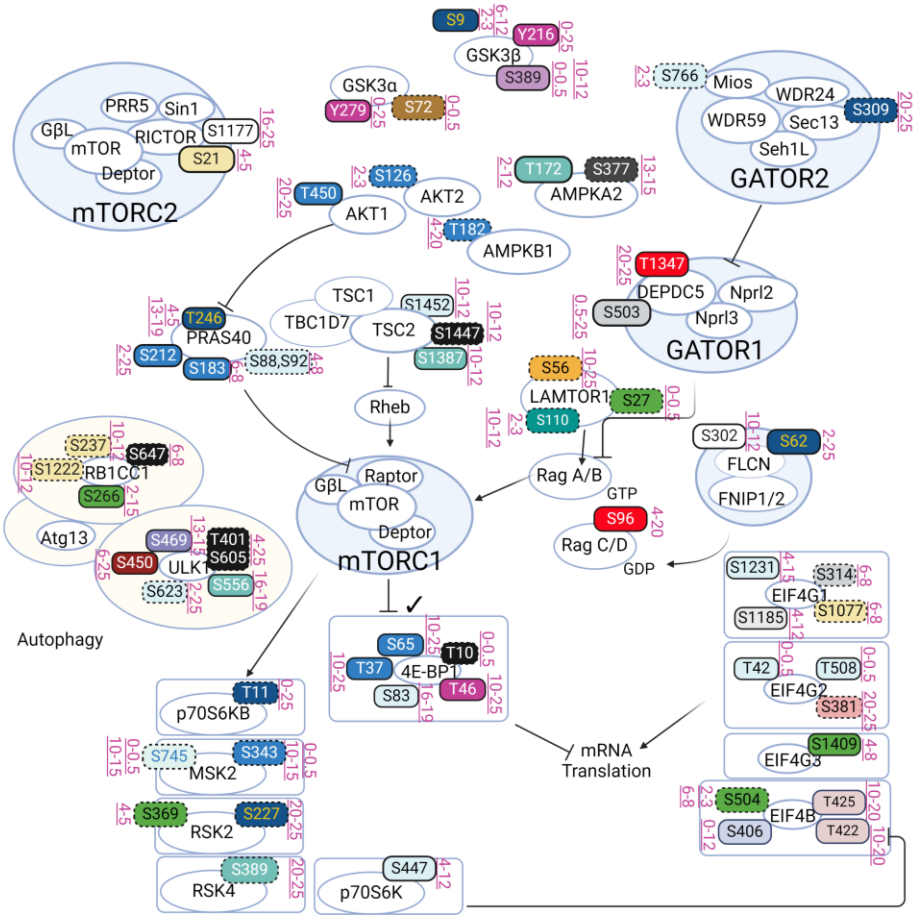

Figure 3

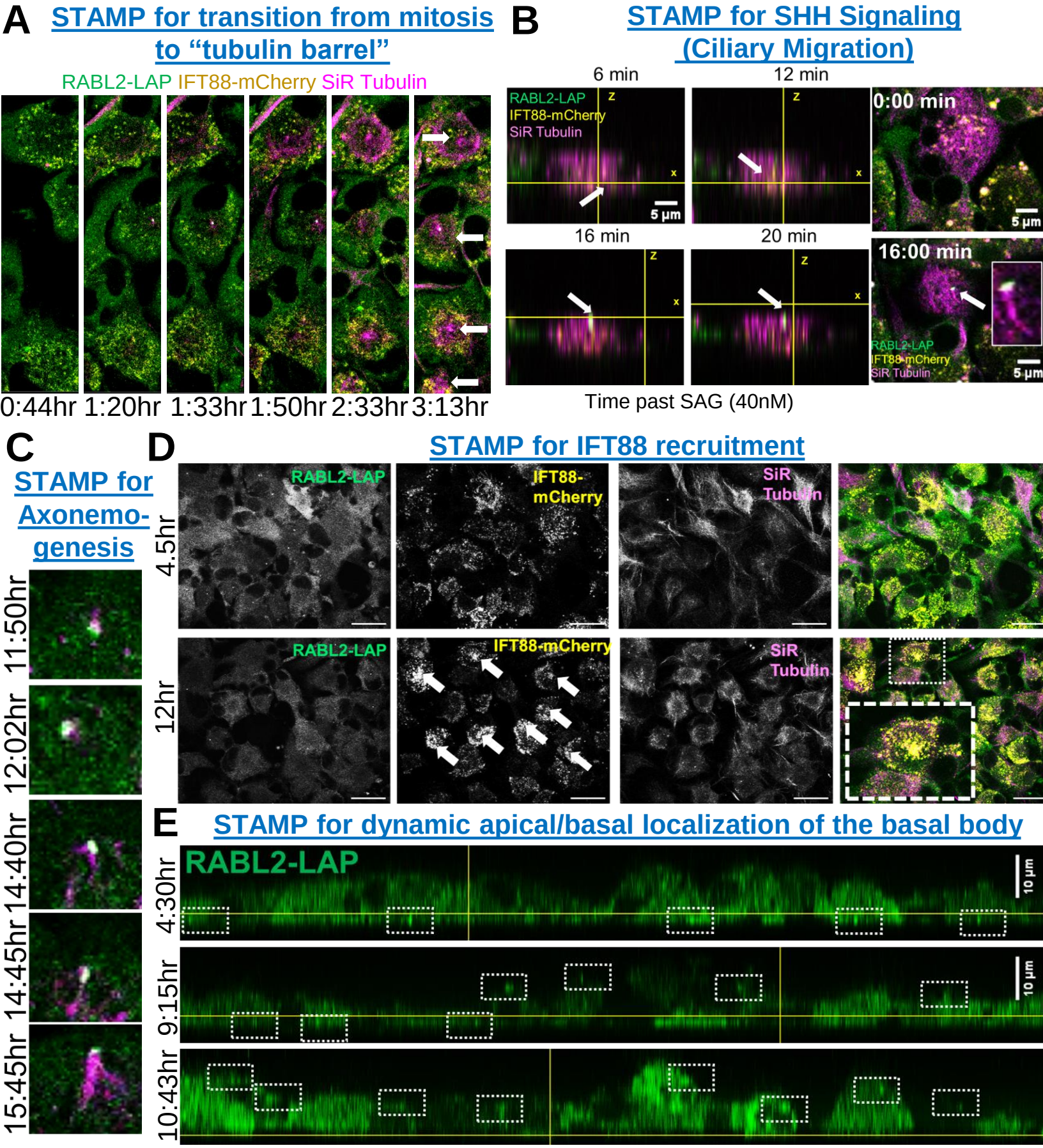
A
STAMP for transition from mitosis to "tubulin barrel"
RABL2-LAP IFT88-mCherry SiR Tubulin
0:44hr 1:20hr 1:33hr 1:50hr 2:33hr 3:13hr
B
STAMP for SHH Signaling (Ciliary Migration)
6 min
12 min
16 min
20 min
RABL2-LAP
IFT88-mCherry
SiR Tubulin
5 µm
0:00 min
16:00 min
Time past SAG (40nM)
C
STAMP for Axonemo-genesis
11:50hr
12:02hr
14:40hr
14:45hr
15:45hr
D
STAMP for IFT88 recruitment
4.5hr
12hr
RABL2-LAP
IFT88-mCherry
SiR Tubulin
E
STAMP for dynamic apical/basal localization of the basal body
4:30hr
9:15hr
10:43hr
RABL2-LAP
10 µm

Figure 4

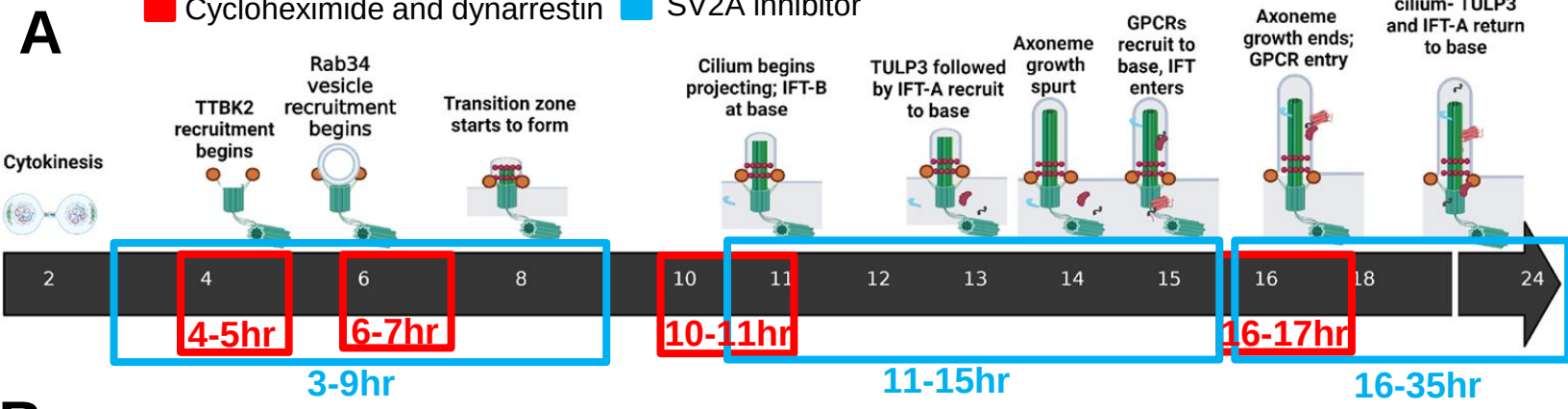

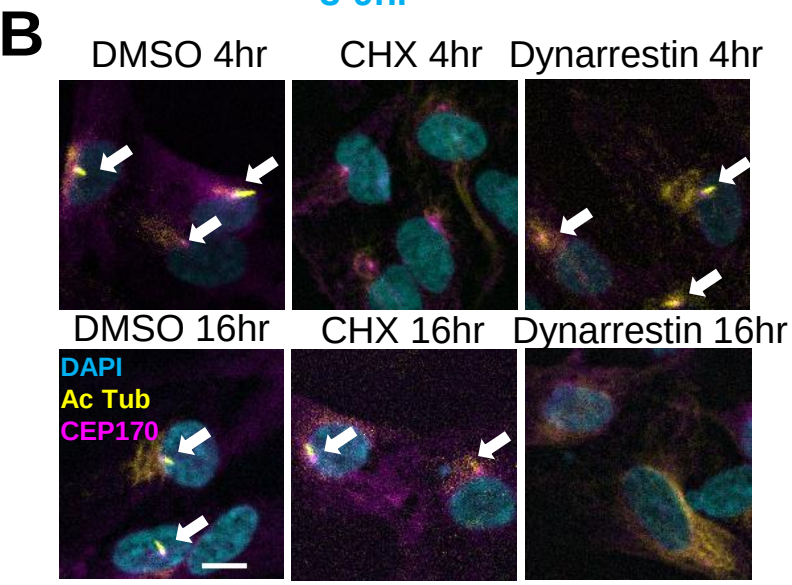

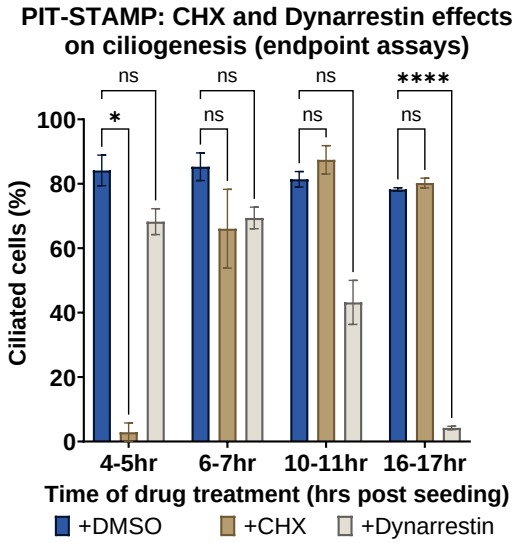

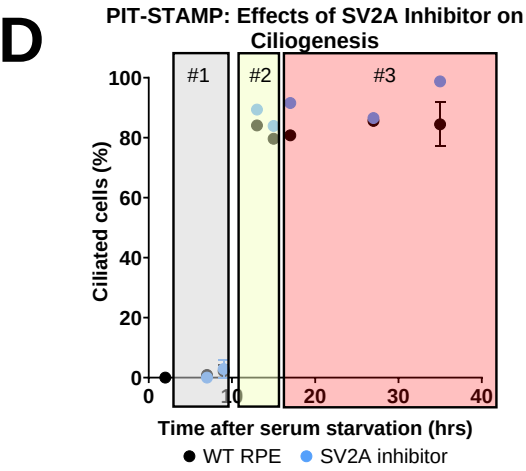

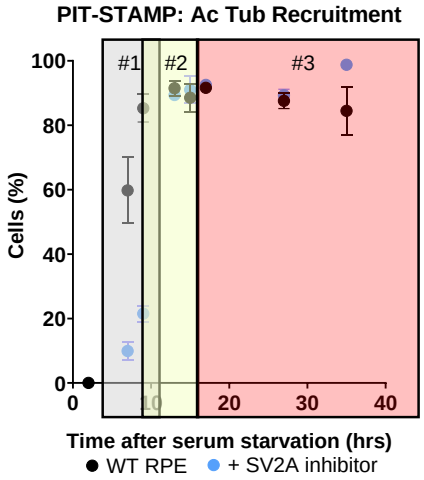

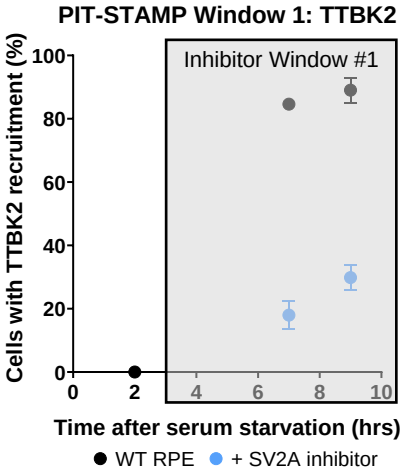

Window 1: Treated between 3-9hr
Window 2: Treated between 11-15hr
Window 3: Treated between 16-35hr

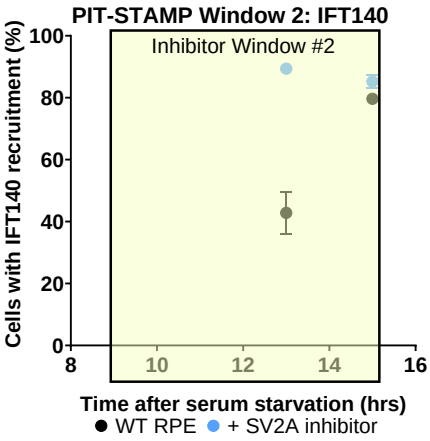

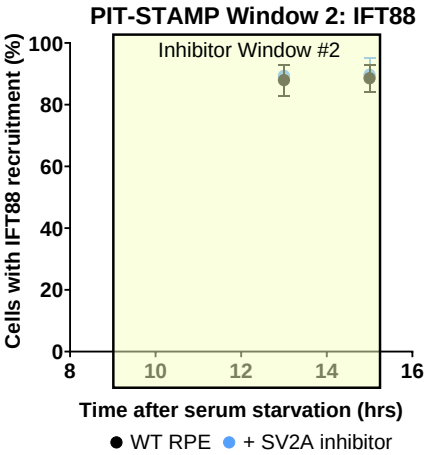

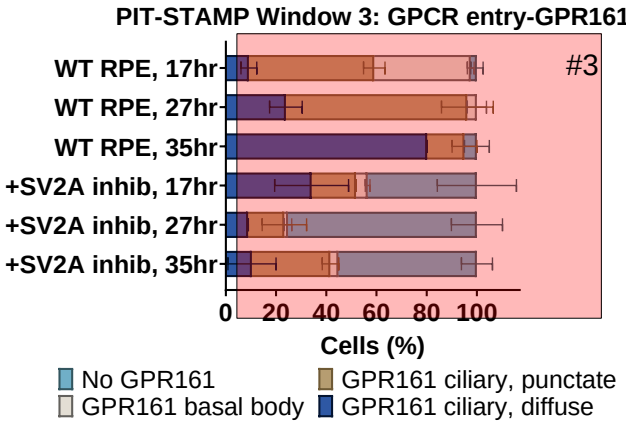

Figure 5

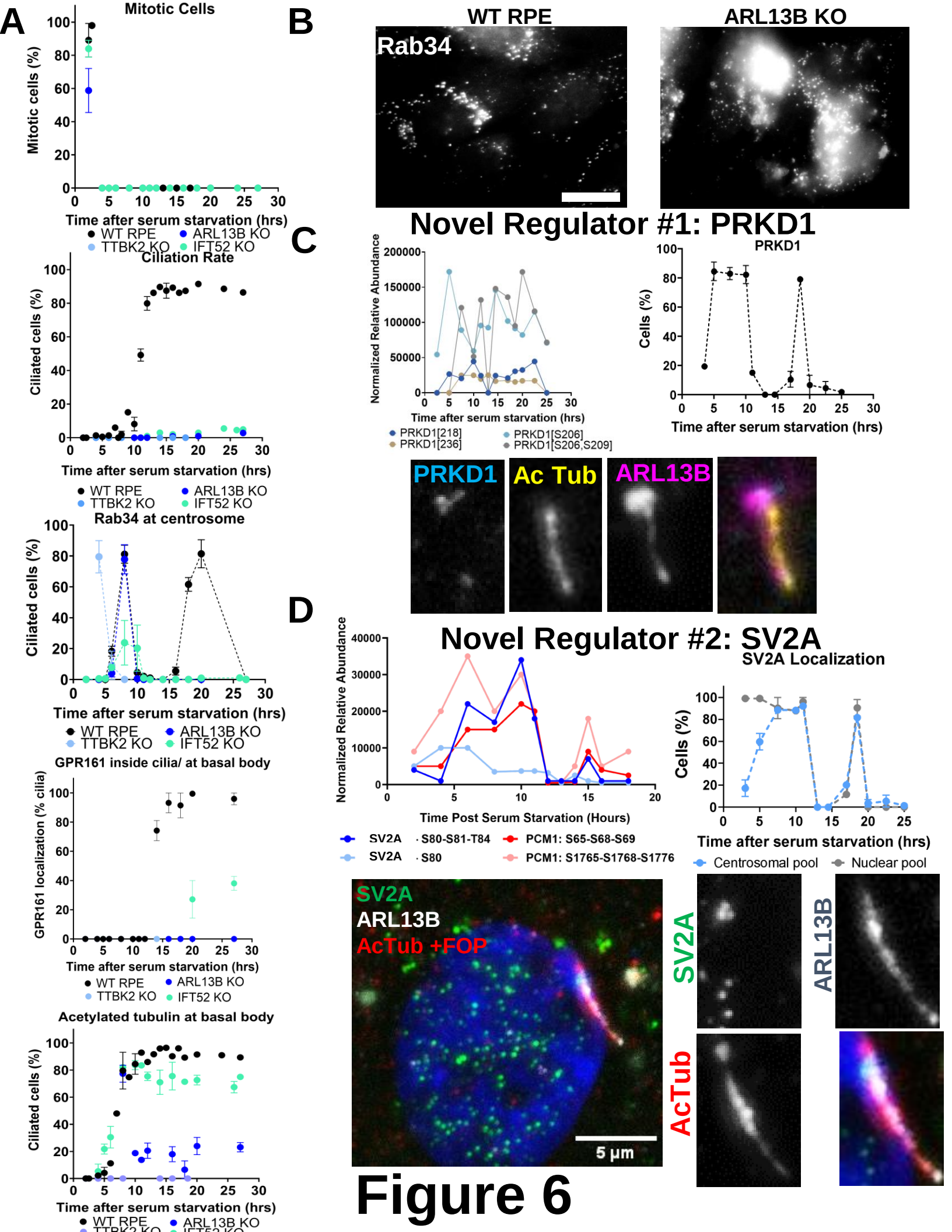
A
Mitotic Cells
Mitotic cells (%)
Time after serum starvation (hrs)
WT RPE
ARL13B KO
TTBK2 KO
IFT52 KO
B
WT RPE
ARL13B KO
Rab34
Novel Regulator #1: PRKD1
Normalized Relative Abundance
Time after serum starvation (hrs)
PRKD1[218]
PRKD1[236]
PRKD1[S206]
PRKD1[S206,S209]
PRKD1
Cells (%)
PRKD1
Ac Tub
ARL13B
C
Ciliation Rate
Ciliated cells (%)
Rab34 at centrosome
D
Novel Regulator #2: SV2A
Normalized Relative Abundance
Time Post Serum Starvation (Hours)
SV2A · S80-S81-T84
SV2A · S80
PCM1: S65-S68-S69
PCM1: S1765-S1768-S1776
SV2A Localization
Centrosomal pool
Nuclear pool
GPR161 inside cilia/ at basal body
GPR161 localization (% cilia)
Acetylated tubulin at basal body
SV2A
ARL13B
AcTub +FOP
5 µm
AcTub

Figure 6